Yang, Y, Bashir, M, Li, C and Wang, J

Investigation on Mooring Breakage Effects of a 5 MW Barge-Type Floating Offshore Wind Turbine Using F2A

Article

Citation (please note it is advisable to refer to the publisher's version if you intend to cite from this work)

Yang, Y, Bashir, M, Li, C and Wang, J (2021) Investigation on Mooring Breakage Effects of a 5 MW Barge-Type Floating Offshore Wind Turbine Using F2A. Ocean Engineering, 233. ISSN 0029-8018

Investigation on Mooring Breakage Effects of a 5 MW Barge-Type Floating Offshore Wind Turbine Using F2A

Yang YANG [a,b,*], Musa BASHIR [b], Chun LI [c], Jin WANG [b]

[a.] Faculty of Maritime and Transportation, Ningbo University, Ningbo, 315211, P.R. China

[b.] Liverpool Logistics, Offshore and Marine (LOOM) Research Institute, Liverpool John Moores University, Liverpool, Byrom Street, L3 3AF, UK

[c.] School of Energy and Power Engineering, University of Shanghai for Science and Technology, Shanghai, 200093, P.R. China

Abstract: Stability and integrity of the station-keeping system are vital to the safety and performance of a floating offshore wind turbine (FOWT). Failure of a mooring line significantly increases the risk of damage to the FOWT. Consequently, it is necessary to investigate the impacts of a mooring breakage on dynamic responses of the rotor, platform and the remaining mooring lines of a FOWT. In order to address the associated research needs of a FOWT subjected to mooring failures, this study has analyzed and predicted the transient behaviors of a 5 MW barge-type FOWT under rated and extreme conditions using a coupling framework based on FAST and AQWA (F2A) when a mooring is subjected to a sudden breakage. It is found that the mooring breakages have a minor impact on the aerodynamic performance and aero-elastic responses of the FOWT, although a notable yaw-deviation of the rotor is caused. The platform sway and yaw motions are significantly influenced by the breakage of an upwind mooring line. Thus, the tension in the remaining adjacent mooring line is increased by as much as 156% and 41.6% under the examined rated and extreme conditions, respectively. The emergency shutdown following the mooring line breakage decreases the platform drift and yaw motions, while the platform pitch motion is enhanced by the shutdown measure due to the absence of aerodynamic damping. In addition, significant reductions in the tensions of upwind mooring lines that suffer the most severe tension are achieved. The shutdown measure is beneficial in ensuring the operational safety of the FOWT subjected to a sudden breakage of a mooring line.

Keywords: Floating offshore wind turbines; Mooring breakage; Fully coupled analysis; Shutdown; Dynamic behavior; F2A.

1 Introduction

Due to the availability of stable wind resources and higher energy capacity, offshore wind is increasingly attracting attention in the development of renewable energy. A recent report by the International Energy Agency (IEA) indicates that the global offshore wind capacity has been consistently expanding by nearly 30% per year since 2010. A moderate forecast shows that the global offshore wind energy market is expecting an annual upswing of 20 GW of newly-installed capacity until 2030 [1]. Since most of the coastal areas with high-quality wind resources are developed, attention has shifted to deeper seas and this has been a subject of research by both academic institutions and industrial organizations. The cost of fixed-bottom offshore wind turbines significantly increases with water depth. Consequently, fixed-bottom is not considered an economically viable option for supporting wind turbines operating in deep waters. Therefore, floating offshore wind turbines (FOWTs) have become a promising technology for the exploitation of wind energy in deeper seas [2].

The most common types of FOWTs include spar, semi-submersible, tension leg platform and barge. The barge-type platform is stabilized by buoyancy and has advantages in reducing the total weight, cost and construction difficulty of the FOWT when compared to the other platforms [3]. Due to its structural simplicity, modelling suitability and commercial viability, a barge-type platform has been widely used in numerous studies for the design of FOWTs [4-9]. Compared to fixed-bottom offshore wind turbines, the coupling between aero-elastic responses and hydrodynamic loads of a FOWT is much more complex. This can be explained in twofold: i) the much larger motion amplitudes of the support system produce significant impacts on the kinematics of the blades, resulting in more complicated aero-elastic responses [10]; ii) a station-keeping system is added to avoid the free-drift motion of the FOWT. This means that the dynamics of the mooring system are coupled with the aero-hydro-servo-elastic responses of the FOWT. In addition to the functionality of station-keeping, the mooring system maintains the platform’s orientation in order to avoid a large yaw-deviation of the rotor [11]. Therefore, the integrity and performance of the mooring system is vital to the stability and safety of a FOWT.

During its service life cycle, a FOWT operates in a harsh marine environment, experiencing both moderate and extreme met-ocean conditions. The mooring system may suffer a failure due to corrosion, extreme gust or accumulated fatigue damage [12]. For such a sudden breakage of mooring line to occur, the platform motions are expected to rapidly increase. As a result, the dynamic responses of the wind turbine will be enhanced. In addition, the position and orientation of the FOWT could be significantly changed and may lead to severe consequences including damage to power cables/umbilicals and drivetrain system. Furthermore, the tension in the remaining mooring lines may exceed the material strength limit, leading to more severe accident events, like collision with other FOWTs due to the large drift motion under the non-moored or weakly-moored states. A sudden breakage of a mooring line endangers the operational safety of the FOWT and produces a high risk of economic loss to the wind farm. Therefore, it is imperative to investigate the mooring breakage effects on the dynamic responses of a FOWT under wind-wave-current loadings.

Numerous studies have been carried out to investigate the consequences and impacts of mooring line breakages on floating platforms. Gao *et al.* [13] investigated the influence of a mooring breakage on the annual extreme tension and fatigue damage of the remaining mooring lines of a TLP. It was found that the extreme tension of the adjacent mooring line is increased by 20% to 30%. In addition, the breakage of a mooring line produces an increase of 50% to 90% in the fatigue damage of the remaining lines. Yang *et al.* [14-16] analyzed the transient responses of a hull-tendon-riser coupled TLP model when a tendon is suddenly disconnected due to accident. The dynamic behavior of the TLP and transient tensions of the remaining tendons are investigated. The quasi-static catenary model was used to predict the tension of the mooring lines. Malayjerdi *et al.* [17] compared the dynamic responses of a TLP under intact and damaged tendon conditions. The static stability of the TLP with one or three broken tendons was investigated.

It is noted that the studies mentioned above focused on the impacts of a mooring system failure for offshore oil and gas platforms. However, there are limited studies relating to research on mooring breakage effects on the fully coupled responses of FOWTs. FOWTs suffer much more severe aerodynamic loads compared to an offshore oil and gas platform. The transient couplings between aerodynamic loads and hydrodynamic responses of a FOWT under a mooring breakage are more complicated due to the larger platform motion experienced after the mooring failure. Bae *et al.* [18] analyzed the performance changes due to a broken mooring line of a 5 MW semi-submersible FOWT. A series of numerical simulations were conducted using an integrated tool, CHARM3D-FAST. The results show that a mooring breakage causes notable nacelle-yaw errors and huge drift of the platform. Consequently, the power-line might be disconnected and successive failure of adjacent FOWTs are likely to occur due to potential collisions. Li *et al.* [19] investigated the transient responses of a spar-type 5 MW FOWT with fractured mooring lines using an in-house simulation tool. A large drift was caused by a mooring failure and the risk of collision between FOWTs was discussed for two different wind farm configurations. However, it is noted that the aerodynamic loads were predicted using a quasi-steady method and the aero-elastic effects of the blades were ignored. Moreover, the memory effects on the free-surface were not examined. Ma *et al.* [20] investigated the dynamic responses of a 5 MW semi-submersible FOWT with a mooring line breakage due to extreme coherent gust using a commercial tool, SIMA. The time length of the extreme gust occurrence was investigated. However, it is noted that a quasi-steady method was used in predicting the aerodynamic loads, implying that the fully coupled aero-hydro-servo-elastic were not well examined. Furthermore, the above studies focused on spar and semi-submersible models, while mooring breakage analysis of a barge concept, another promising technology for floating wind energy extraction, has not been performed yet. In addition, the resilience of the FOWT can be enhanced by installing more than a mooring for each fairlead to avoid collision to its adjacent platforms under mooring breakage scenarios.

In order to address the limitations resulting from the above reviewed studies, this paper aims to investigate the mooring breakage impacts on the fully coupled dynamic responses of a FOWT. The widely-used barge-type NREL 5 MW FOWT [21] is adopted for the case study. A novel coupling framework (F2A) based on FAST [22] and AQWA is developed and implemented to conduct aero-hydro-servo-elastic simulations of the FOWT with intact and broken mooring lines. The dynamic behaviors of the FOWT under a sudden breakage of different mooring lines are obtained using F2A. In addition, the effects of an emergency shutdown following the mooring breakage are investigated.

In the subsequent section, the barge model and its mooring system are briefly described. Afterwards, detailed descriptions of the methodologies used for the development of F2A are presented. A comparison against OpenFAST is then carried out for the validation of F2A. In Section 3, the fully coupled dynamic responses of the FOWT under the intact and broken mooring line scenarios are obtained and then compared. In addition, the impact of a shutdown measure following a mooring breakage is discussed in Section 4. The main findings and conclusions of this study are presented in Section 5.

2 Fully coupled modelling of the FOWT

2.1 The ITI barge concept

The barge model developed by ITI Energy, which has been used in numerous studies [4-9] for the design of FOWTs due to its structural simplicity and modelling suitability, is adopted to conduct the case study. The buoyancy-stabilized ITI barge model was initially designed to support a hybrid floating energy system that is composed of a wind turbine and an oscillating water column (OWC) wave-power device. The ITI barge has a square geometry that reduces the manufacturing difficulty of the platform. The barge has a square moon pool in the middle for deployment of the OWC wave-power device which connects to the bottom of the tower. A mooring system consisting of eight catenary lines was designed for the station-keeping of the barge model. The mooring lines are symmetrically attached to the four corners of the barge. Table 1 presents a summary of the properties of the ITI barge and its mooring system [21]. A schematic diagram of the NREL 5 MW wind turbine mounted on the ITI barge is presented in Fig. 1.

Table 1: Summary of the properties of the ITI barge and its mooring system

Property	Value/Unit
Barge size	40 m × 40 m × 10 m
Moon pool size	10 m × 10 m × 10 m
Draft	4.0 m
Mass	5.452×10^6 kg
Center of mass	(0.0, 0.0, -0.2818 m)
Roll Inertia	7.269×10^8 kg·m^2
Pitch Inertia	7.269×10^8 kg·m^2
Yaw Inertia	1.4539×10^9 kg·m^2
Water depth	150
Anchor radius	423.422 m
Unstretched line length	473.3 m
Line diameter	0.809 m
Line mass density	130.4 kg/m
Line extensional stiffness	5.890×10^8 N
Line type	R4-studless
Breaking load	4420.6 kN

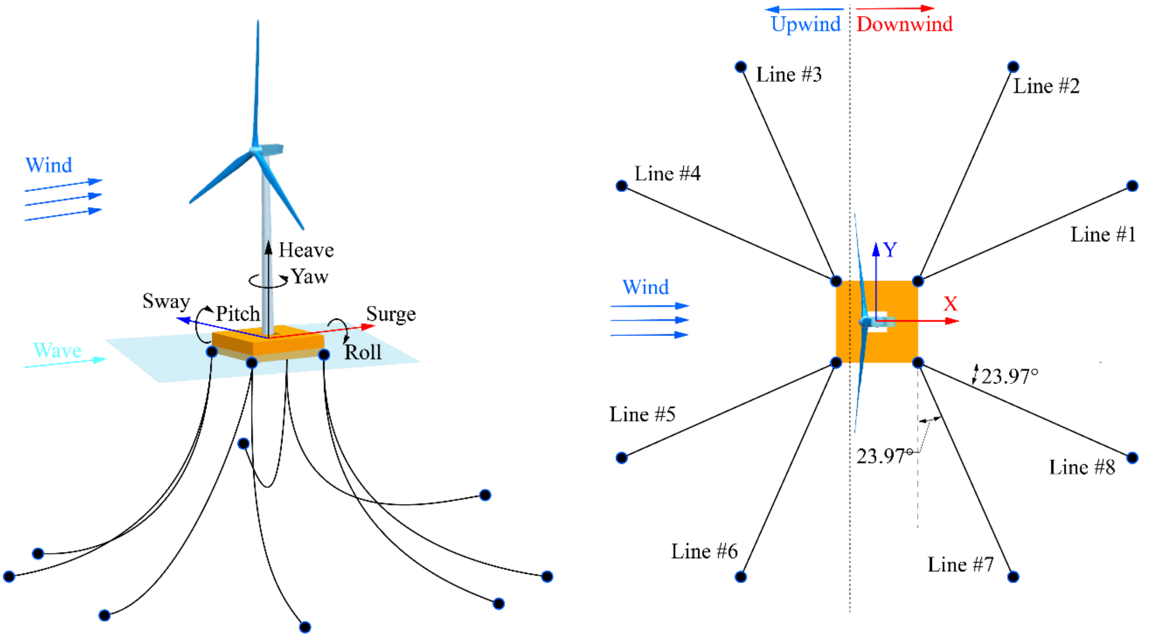

Fig.1: The NREL 5 MW wind turbine supported by the ITI barge model

2.2 Dynamic modelling of mooring lines

The mooring lines are commonly modelled as a quasi-static catenary when developing a fully coupled model of a FOWT [24-26]. This means that the tension in the mooring lines is determined for a known fairlead position by assuming that the cables are in static equilibrium for any given instant. However, the inertial effects of the cables and dynamic effects from the platform motions cannot be examined. As revealed in the studies by Hall *et al.* [27-28], the quasi-static method underestimates the tension of mooring lines, while the tension obtained using a dynamic modelling approach agrees quite well with the experimental results of a semi-submersible FOWT. For an accurate prediction of the dynamic responses of the FOWT subjected to a sudden mooring breakage, a dynamic modelling approach needs to be used in the calculation of mooring line tensions instead of the quasi-static catenary method. Fig. 2 presents a schematic diagram of the dynamic model of a mooring line. In the figure, S_j is the unstretched length between the anchor and the j^{th}-node of the mooring line, D_e is the diameter of the local segment of the mooring line.

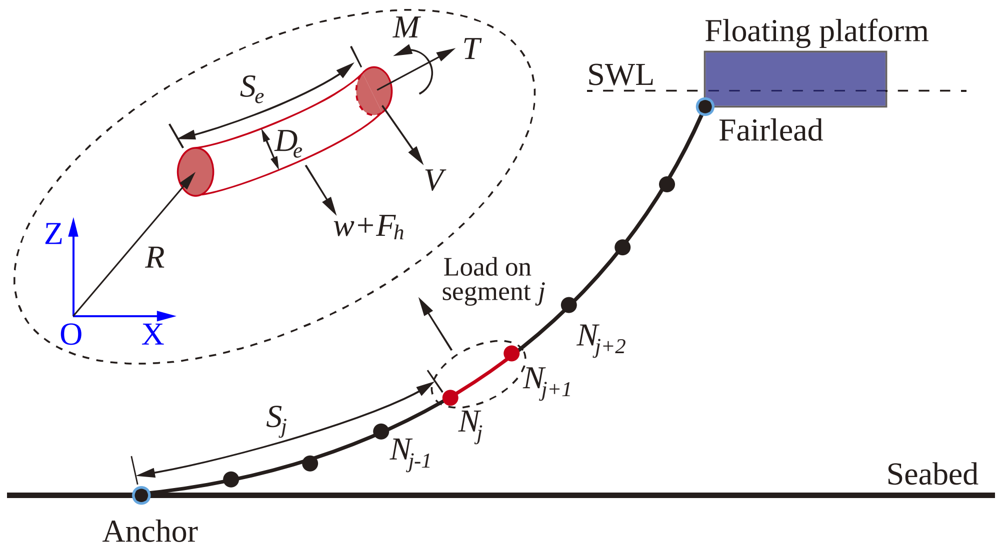

Fig. 2: Schematic diagram of the dynamic model of a mooring line

Each of the mooring lines is modelled as a chain of Morison-type elements subjected to various external forces. The equation of motion of an arbitrary element of the mooring line is presented as follows [29]:

$$\begin{cases} \dfrac{\partial \mathbf{T}}{\partial S_e} + \dfrac{\partial \mathbf{V}}{\partial S_e} + \boldsymbol{w} + \boldsymbol{F}_h = m_e \dfrac{\partial^2 \mathbf{R}}{\partial t^2} \\ \dfrac{\partial \mathbf{M}}{\partial S_e} + \dfrac{\partial \mathbf{R}}{\partial S_e} \times \mathbf{V} = -\mathbf{q} \end{cases} \tag{1}$$

where **T** and **V** are, respectively, the tension force and shear force vectors at the first node of the element; **R** is the position vector of the first node of the cable element; S_e is the unstretched length of the element; $\boldsymbol{w}$ and $\boldsymbol{F}_h$ are, respectively, the weight and hydrodynamic load vectors per unit length of the element; m_e is the mass per unit length. $\mathbf{M}$ is the bending moment vector at the first node of the element; $\mathbf{q}$ is the distributed moment load per unit length of the element.

The bending moment and tension are denoted as follows:

$$\begin{cases} \mathbf{M}=EI\cdot\dfrac{\partial\mathbf{R}}{\partial S_e}\times\dfrac{\partial^2\mathbf{R}}{\partial S_e^2} \\ \mathbf{T}=EA\cdot\varepsilon \end{cases} \tag{2}$$

where EI and EA are the bending stiffness and axial stiffness of the mooring line, respectively.

It is noted that the solution of the mooring tension is fully coupled with platform motions. This means that the effects of the mooring mass, drag forces, inline elastic tension and bending moment are examined.

2.3 Development of F2A coupling framework

In order to obtain the fully coupled dynamic responses of the FOWT subjected to a mooring line breakage, the aero-servo-elastic simulation capabilities of FAST tool are implemented within the hydrodynamic analysis tool (AQWA) through a coupling framework. The coupling framework uses the capabilities of FAST in predicting aero-servo-elastic responses and the advantages of AQWA in modelling nonlinear hydrodynamics and mooring dynamics of a FOWT. Therefore, the coupling framework is called FAST2AQWA, simplified as F2A.

The coupling between hydrodynamic loads and the aero-servo-elastic responses within F2A is achieved through a DLL (*user_force.dll*) that is built in AQWA for calculating the external forces of a floating system. The source code is fully modified to implement the aero-servo-elastic simulation capabilities of a FOWT. In a time-domain analysis performed in AQWA, the DLL is invoked by the AQWA solver to obtain the external force and added-mass. In each invocation, the AQWA program provides the kinematics of the platform to the DLL for updating the kinematics of the upper structures including the rotor, nacelle and tower. The equations of motion of the upper structures are solved within the DLL and the tower-base loads are obtained. With an appropriate transformation, the tower-base loads are passed into the AQWA program as the external force item. Following this, the equation of motion of the platform given in Eq. (3) [30] is solved and the platform acceleration vector is then obtained.

$$(\boldsymbol{m}+\boldsymbol{A}_{\infty})\ddot{\boldsymbol{X}}(t)+\boldsymbol{C}\dot{\boldsymbol{X}}(t)+\boldsymbol{K}\boldsymbol{X}(t)+\int_0^t \boldsymbol{h}(t-\tau)\ddot{\boldsymbol{X}}(\tau)\mathrm{d}\tau=\boldsymbol{F}_{\mathrm{h}}(t)+\boldsymbol{F}_{\mathrm{t}}(t)+\boldsymbol{F}_{\mathrm{e}}(t) \tag{3}$$

where $\boldsymbol{m}$ is the inertial mass matrix of the platform, $\boldsymbol{A}_{\infty}$ is the added-mass matrix at the infinite wave frequency, $\boldsymbol{K}$ and $\boldsymbol{C}$ are, respectively, the total stiffness and damping matrices; $\boldsymbol{X}(t)$, $\dot{\boldsymbol{X}}(t)$ and $\ddot{\boldsymbol{X}}(t)$ are, respectively, the displacement, velocity and acceleration vectors of the platform; $\boldsymbol{h}(t)$ is the acceleration impulse function matrix used to examine the radiation memory effects; $\boldsymbol{F}_{\mathrm{h}}(t)$ and $\boldsymbol{F}_{\mathrm{t}}(t)$ are, respectively, the total hydrodynamic and mooring load vectors acting on the platform; $\boldsymbol{F}_{\mathrm{e}}(t)$ is the external force vector obtained through the DLL.

Fig. 3 presents a flowchart of F2A to illustrate the coupling between the responses of the upper structures and the platform. The aero-servo-elastic simulation capabilities of FAST are fully implemented within the DLL that will be invoked by the AQWA program. The simulations are carried out using AQWA and independent of the FAST program. As presented in Fig. 3, a simulation is examined by the following steps:

(1) Initialize the platform responses in the AQWA program.

(2) Invoke the user-force.dll to update the kinematics of tower, nacelle and blades.

(3) Calculate aerodynamic loads on the blades based on the wind data under the consideration of the servo-control scheme and the elasticity of the wind turbine.

(4) Transfer the tower-base loads obtained in the user-force.dll into the AQWA program.

(5) Compute the platform acceleration by solving Eq. (3) based on the tower-base loads from the DLL, hydrodynamic loads and mooring restoring forces on the platform.

(6) Repeat steps (2)~(5) until the termination of the simulation.

It is apparent that the platform responses are influenced by the aerodynamic loads on the blades and tower as well as their elastic responses, and vice versa. The fully coupled aero-hydro-servo-elastic model of a FOWT is established within AQWA program through the DLL.

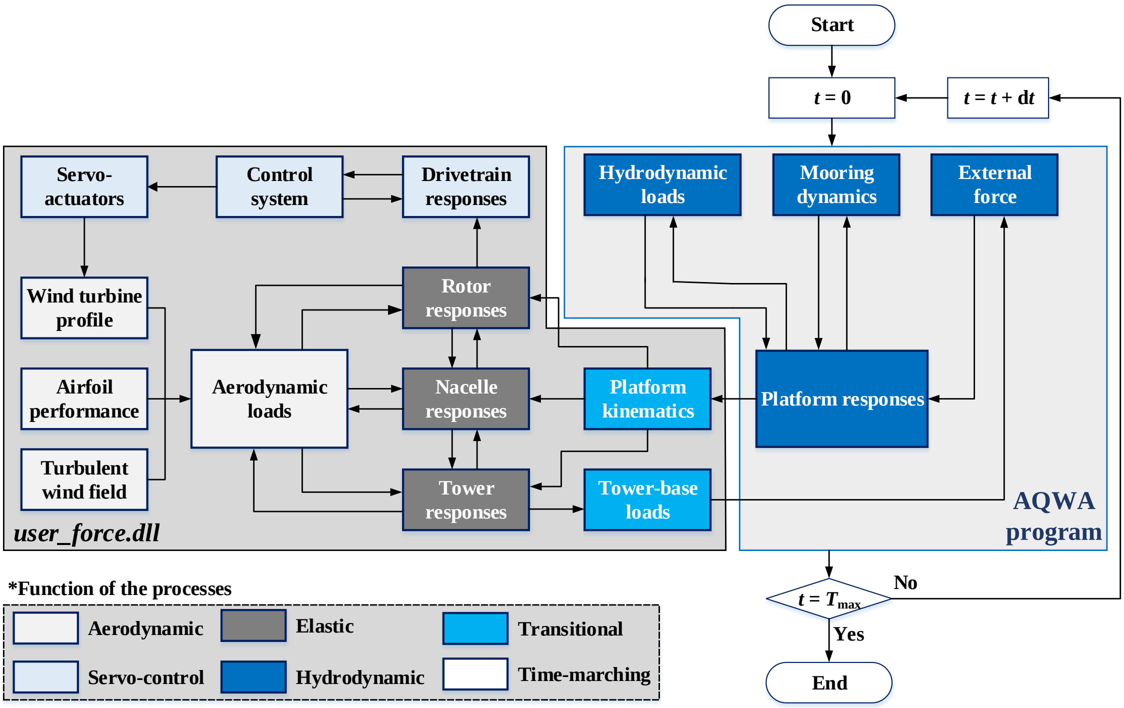

Fig. 3: Flowchart of the F2A framework

It is noted that the transitional results calculated directly by the AQWA program and DLL are referred to different coordinate systems. To be more specific, the platform displacement, velocity and acceleration produced directly by the AQWA program are the responses at the center of mass referred with the inertial coordinate system. However, the kinematics of the upper structures are corrected by using the responses at the reference point that are referred with the platform's local coordinate system. Similarly, the tower-base loads obtained by the DLL are referred to the platform's local coordinate system and they act at the tower-base, but the external forces used in AQWA program are referred to the inertial coordinate system and they act at the center of mass of the platform. Therefore, transformations are needed to apply on the transitional results to examine the coupling correctly.

The transformation matrix, $\mathbf{T}_{\text{mat}}$, given in Eq. (4) is used to correct the platform displacement vector.

$$\mathbf{T}_{\text{mat}} = \begin{bmatrix} \dfrac{\theta_1^2\sqrt{1+s}+\theta_2^2+\theta_3^2}{s\sqrt{1+s}} & \dfrac{\theta_3 s+\theta_1\theta_2(\sqrt{1+s}-1)}{s\sqrt{1+s}} & \dfrac{-\theta_2 s+\theta_1\theta_3(\sqrt{1+s}-1)}{s\sqrt{1+s}} \\ \dfrac{-\theta_3 s+\theta_1\theta_2(\sqrt{1+s}-1)}{s\sqrt{1+s}} & \dfrac{\theta_2^2\sqrt{1+s}+\theta_1^2+\theta_3^2}{s\sqrt{1+s}} & \dfrac{\theta_1 s+\theta_2\theta_3(\sqrt{1+s}-1)}{s\sqrt{1+s}} \\ \dfrac{\theta_2 s+\theta_1\theta_3(\sqrt{1+s}-1)}{s\sqrt{1+s}} & \dfrac{-\theta_1 s+\theta_2\theta_3(\sqrt{1+s}-1)}{s\sqrt{1+s}} & \dfrac{\theta_3^2\sqrt{1+s}+\theta_1^2+\theta_2^2}{s\sqrt{1+s}} \end{bmatrix} \tag{4}$$

where θ_1, θ_2 and θ_3 are, respectively, the roll, pitch and yaw angles of the platform. s is equal to $\theta_1^2+\theta_2^2+\theta_3^2$.

When the platform reference point is defined as the origin of the inertial coordinate system, *i.e.* (0, 0, 0), the platform displacement vector is corrected as follows:

$$\mathbf{D}_{\text{DLL}} = \mathbf{D}_{\text{AQWA}} - \mathbf{T}_{\text{mat}} \cdot \mathbf{CoG} \tag{5}$$

where $\mathbf{CoG}$ is the position vector from the reference point to the mass center of the platform. $\mathbf{D}_{\text{AQWA}}$ and $\mathbf{D}_{\text{DLL}}$ are the platform displacement vectors obtained in AQWA and the one passed into the DLL, respectively.

The translational velocity vector of the platform is corrected as follows:

$$\mathbf{U}_{\text{DLL}} = \mathbf{U}_{\text{AQWA}} - \mathbf{T}_{\text{mat}} \cdot \mathbf{CoG} \times \boldsymbol{\omega} \tag{6}$$

where $\mathbf{U}_{\text{AQWA}}$ and $\mathbf{U}_{\text{DLL}}$ are the platform velocity vectors obtained in AQWA and the one used in the DLL, respectively; $\boldsymbol{\omega}$ is the rotational velocity vector of the platform obtained in AQWA.

A predictor-corrector time-marching algorithm is adopted for solving the equations of motion of the upper structures, the acceleration vector obtained in the predictor stage will be used in the corrector stage for the final solution. It means that the platform acceleration vector is also essential for the correction of the kinematics of the upper structures. However, the platform acceleration is an unknown item until the complete solving of the equation of motion in the AQWA program at the current time step. Therefore, the platform acceleration vector is estimated numerically in the DLL based on the velocity vectors at the last and current time steps as follows:

$$\mathbf{a}_{\mathrm{DLL}} = (\mathbf{U}_{\mathrm{DLL}} - \mathbf{U}'_{\mathrm{DLL}}) / \mathrm{d}t \tag{7}$$

where $\mathbf{a}_{\mathrm{DLL}}$ is the platform acceleration and $\mathbf{U}'_{\mathrm{DLL}}$ is the platform velocity at the last time step, dt is the time step of the simulation.

Similarly, the tower-base loads obtained directly in the DLL are transformed as follows:

$$\mathbf{F}_{\mathrm{AQWA}} = \mathbf{T}_{\mathrm{mat}}^{-1} \cdot \mathbf{F}_{\mathrm{DLL}} \tag{8}$$

$$\mathbf{M}_{\mathrm{AQWA}} = \mathbf{T}_{\mathrm{mat}}^{-1} \cdot (\mathbf{M}_{\mathrm{DLL}} - \mathbf{CoG} \times \mathbf{F}_{\mathrm{DLL}}) \tag{9}$$

where $\mathbf{F}_{\mathrm{AQWA}}$ and $\mathbf{F}_{\mathrm{DLL}}$ are the translational force vectors in the AQWA program and DLL, respectively. $\mathbf{T}_{\mathrm{mat}}^{-1}$ is the inverse matrix of $\mathbf{T}_{\mathrm{mat}}$. $\mathbf{M}_{\mathrm{AQWA}}$ used in AQWA is the moment vector acting at the platform's mass center with respect to the inertial coordinate system. $\mathbf{M}_{\mathrm{DLL}}$ obtained in the DLL is the moment vector acting at the tower-base with respect to the platform's local coordinate system.

2.3 Validation of F2A

FAST was developed by NREL for aero-hydro-servo-elastic coupled analysis of horizontal axis wind turbines. FAST has been verified and approved as a reliable numerical tool for the analysis of wind-wave coupled loads on wind turbines by Germanischer Lloyd. In addition, FAST was used as the main numerical tool in numerous international projects including the OC3 project, a collaborative study with focus on validation and improvement of numerical tools for wind turbine analysis. The numerical predictions from FAST agreed well with the experimental data for the OC3-Hywind [31] and DeepCwind semi-submersible concepts[32]. Since FAST has been well validated by experimental data in numerous studies, it is agreed that the tool is capable of producing accurate and reliable numerical simulation results of FOWTs under wind-wave coupled conditions. OpenFAST, the latest version of FAST, is therefore used to validate the coupled model developed in this study.

The newly-developed tool F2A is validated through comparisons against OpenFAST. The dynamic responses of the NREL 5 MW wind turbine supported by the ITI barge platform under a turbulent wind condition are predicted by these two tools and then compared. Following the IEC 61400-3 standard regarding the definition of design load case 1.1 for normal power production, the normal turbulence model (NTM) is used to generate the inflow wind. The average wind speed at the hub-height is 11.4 m/s. The corresponding significant wave height and spectral peak period are respectively set to 1.77 m and 7.51 based on the measured met-ocean data of a specific site in the northern coast of Scotland [33]. The control scheme corresponding to normal operation is adopted to adjust rotor speed and blade pitch.

Fig. 4 presents the coupled responses of the FOWT predicted using F2A and OpenFAST. The overall agreements between the results obtained using these two tools are well acceptable. It is observed that the rotor speed calculated by F2A follows the same variation trend and with almost the same values over the entire simulation as OpenFAST. The comparisons offer negligible differences between the results from these tools. The aero-elastic responses of the blade predicted by F2A agree reasonably well with those obtained by OpenFAST, although some minor discrepancies are observed. Similarly, the platform pitch calculated by these two tools follows the same variation trend but with slight differences in magnitude. The discrepancies in the results are mainly caused by the inherent differences between the two tools in how they model the mooring system. Although both AQWA and OpenFAST predict hydrodynamic loads of the platform based on the potential flow theory solvers, natural deviations could be produced due to numerically induced computational errors. Another contribution to the discrepancy is from the time-marching algorithm. AQWA uses a second-order predictor-corrector algorithm for time-marching solutions; however, OpenFAST adopts the 4th-order Rugge-Kutta integration method for the first four time steps and the 4th-order Adams-Beshforth-Mounton predictor-corrector method for the remaining time steps. Since AQWA and OpenFAST use different time integration methods, it is reasonable to expect minor differences between their final results. Nonetheless, the agreements between the results observed from the comparisons are generally very good and they indicate that the aero-servo-elastic simulation capabilities have been well implemented within AQWA through the DLL. It means that F2A is capable of performing a high-fidelity fully coupled analysis of FOWTs.

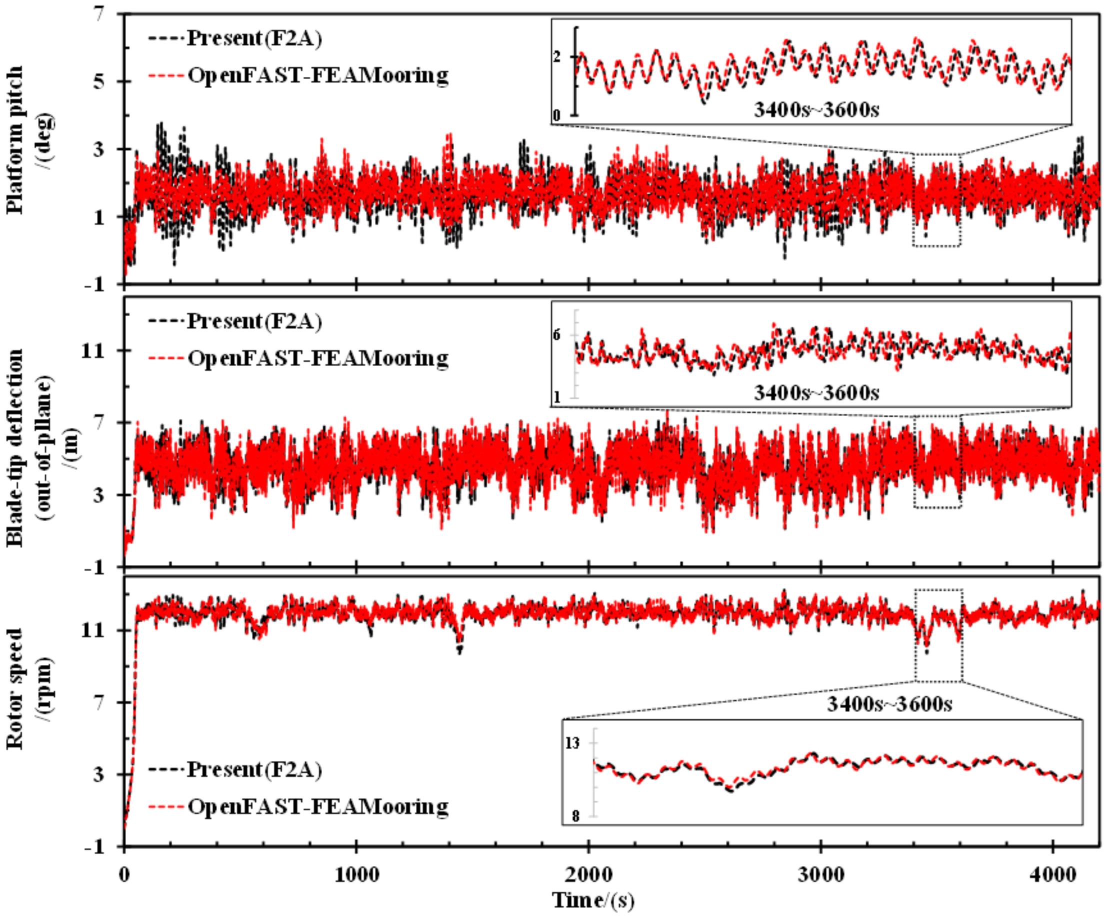

Fig. 4: Comparison between coupled responses of OpenFAST and F2A

In order to confirm the accuracy of F2A in modelling the mooring dynamics, tensions in the mooring lines are obtained through three different modules (FEAMooring, MoporDyn and MAP)in OpenFAST for comparison against F2A. In the FEAMooring module, the mooring lines are modelled using the finite element method to examine mooring's dynamics. The MoorDyn module uses the lumped-mass method for accounting the dynamics of mooring lines. The MAP module employs the quasi-static method in computing the mooring tension. Tensions in the mooring lines predicted using OpenFAST and F2A are presented in Fig. 5. It is found that the mooring tension predicted by each numerical tool follows the same trend. The variation of the results obtained using MAP is smoother than the results from other tools, since the quasi-static method is incapable of accurately capturing the mooring dynamics. The results obtained using F2A agrees well with the results from FEAMooring, since these two tools both employ the finite element method in modelling the mooring lines. The tension in mooring line #6 predicted using MoorDyn is slightly smaller than the results from FEAMooring and F2A. This is because the lumped-mass method used in MoorDyn is incapable of accounting the bending stiffness of the mooring line.

Fig. 5 (b) and Fig. 5(c) present the statistics of mooring tension predicted by OpenFAST and F2A tools. It is noted that the difference between the mean tensions of these tools is insignificant for each mooring line. The maximum tension of each mooring line obtained using F2A is close to those predicted by OpenFAST, although MoorDyn has a slightly larger maximum tension in lines #4 and #5. The results indicate that the mooring model used in F2A can be used to accurately predict tension of mooring lines and capture their dynamics.

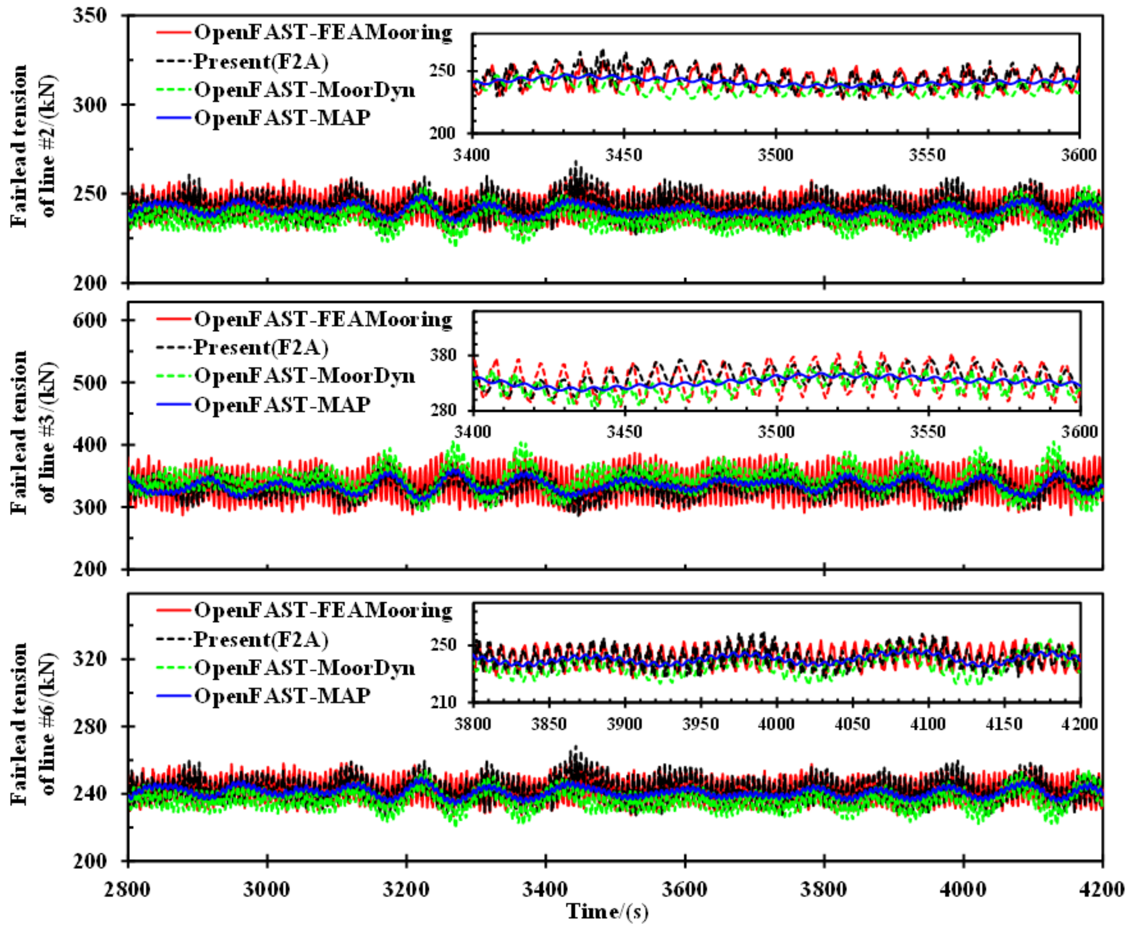

(a) Tension time series

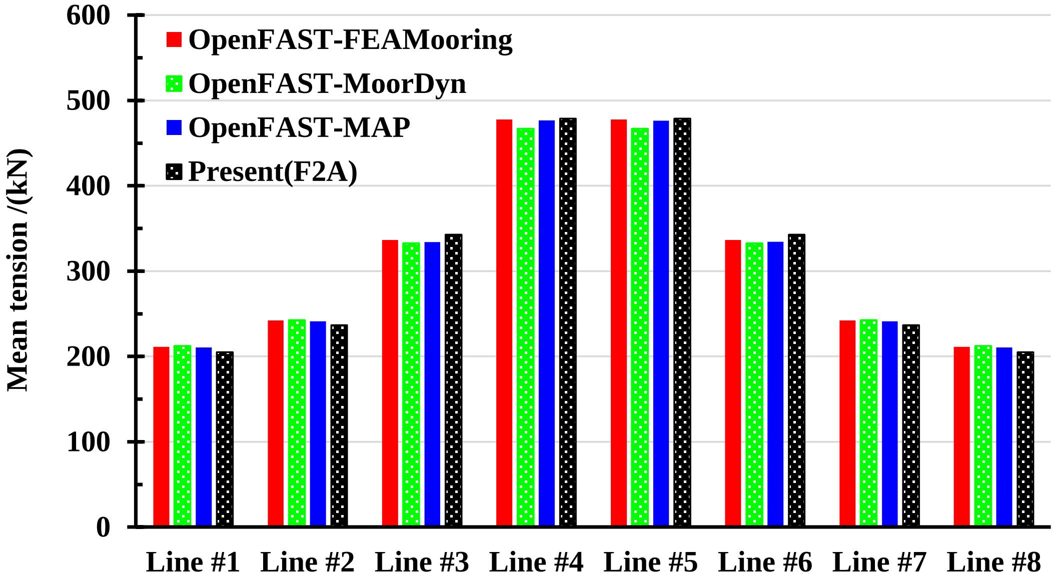

(b) Mean tension

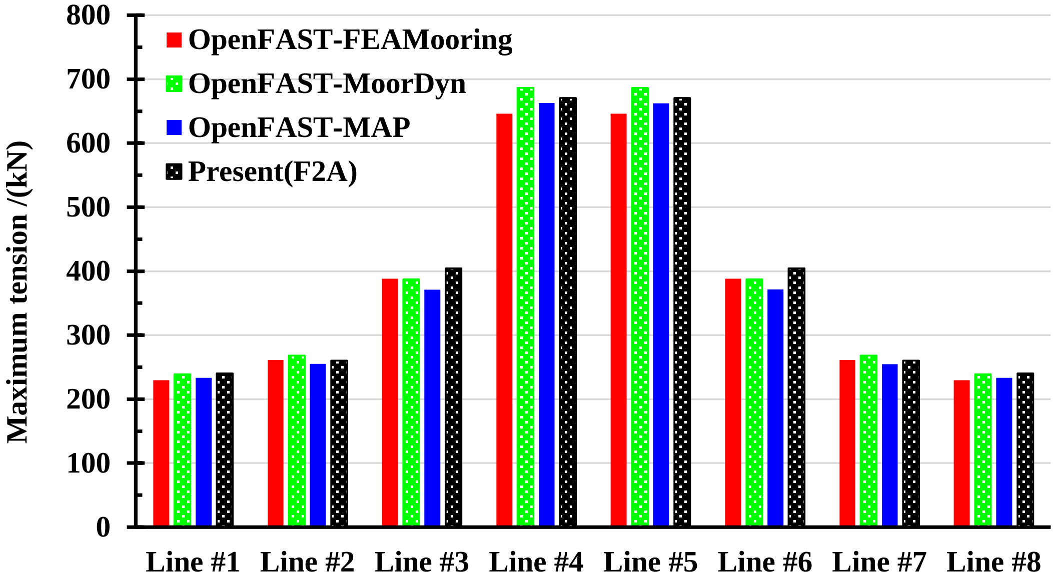

(c) Maximum tension

Fig. 5: Tension in the mooring lines predicted using OpenFAST and F2A

3 Effects of mooring line breakages under the in-operation state

3.1 Load cases and environmental conditions

Based on the met-ocean data of a specific site off the northern-coast of Scotland [33], the significant height and spectral peak period of the irregular wave corresponding to the rated wind speed (11.4 m/s) are selected as 1.786 m and 7.505 s, respectively. The wind turbine is under operational state for normal power production. Fig. 6-(a) presents the wind field generated using TurbSim [34] based on the Kaimal wind spectrum and NTM wind model. The time-varying wave height of the irregular wave, generated based on the P-M wave spectrum, is presented in Fig. 6-(b).

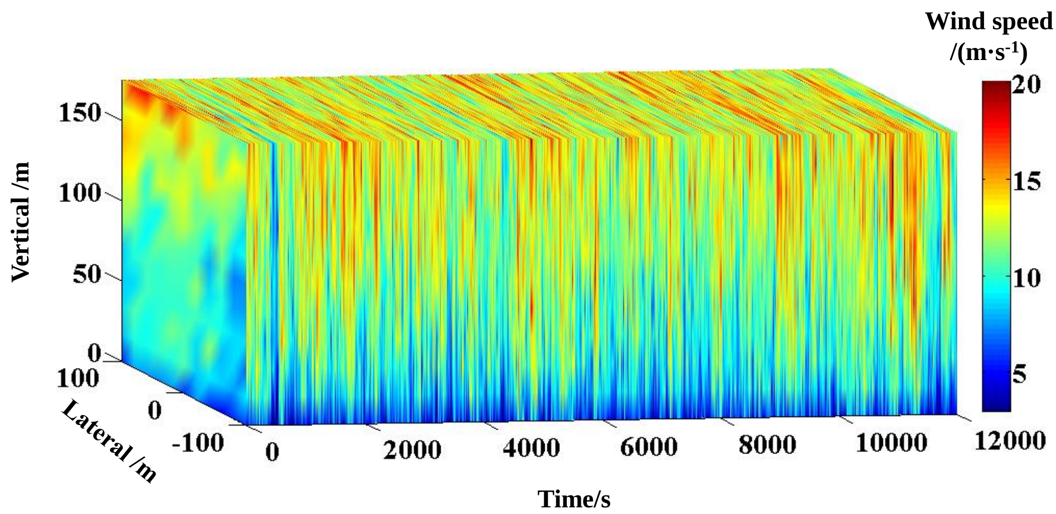

(a) Wind speed of the full-field turbulent wind

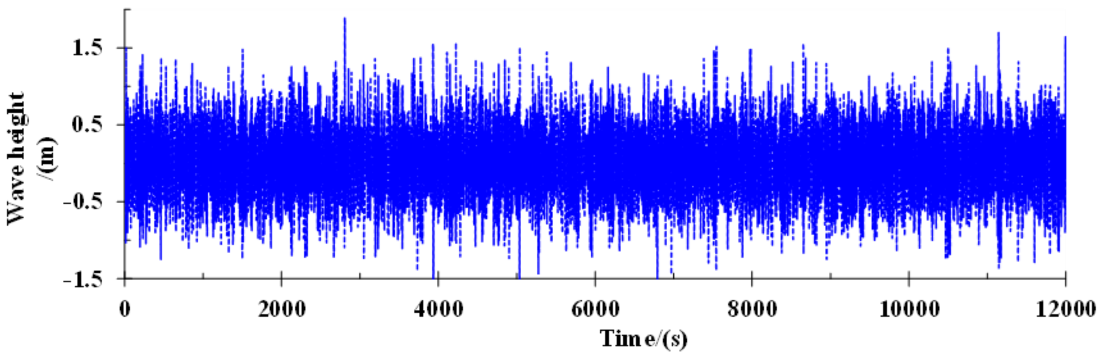

(b) Wave height time series

Fig. 6: Wind speed of the turbulent wind field and wave height of the irregular wave

Since the eight mooring lines are placed symmetrically around the wind turbine, four scenarios of a potential mooring breakage are examined. Specifically, the dynamic responses of the FOWT with a breakage on mooring lines #1, #3, #5 and #7 are examined, respectively. For each simulation, the overall duration is 12000 s and the occurrence time of the breakage is set at 3000th s to allow the completion of the transient behaviors. The breakage means that the mooring line snaps and disconnects from the platform at the specific instant in time. In addition, an intact state of the mooring system is examined for comparisons.

3.2 Effects of mooring line breakages on the dynamic responses

The time-varying results corresponding to the breakages on mooring lines #1 and #5 are presented and discussed in this section. The dynamic responses of the rotor under the intact state and two mooring breakage scenarios are presented in Fig. 7. It is found that the difference between the blade-tip deflections of the intact and broken mooring scenarios is minor. Similar results are obtained for the rotor thrust and generator power. Although the generator power decreases immediately after the breakage on mooring line #5, it recovers to the level of intact state within 100 s. This means that the impact of a mooring breakage on the aerodynamic performance of the rotor is insignificant. It is noted that the mooring breakage has a notable influence on the relative inflow direction, which denotes the intersecting angle between the inflow wind and the longitudinal plane and is also called the “yaw-deviation”. The changes in value of relative inflow direction are caused by the platform yaw motion due to the restoring stiffness reduction of the station-keeping system. Moreover, it is found that the breakage on mooring line #5 leads to a larger yaw-deviation compared to the results corresponding to the breakage on mooring line #1. This is because mooring line #5 is placed in the upwind direction and mooring line #1 is attached in the downwind direction. For the equilibrium condition with a large platform drift, the upwind mooring lines are stretched while the downwind mooring lines are in a loose state. As a result, upwind mooring lines undertake larger loads in keeping the platform in equilibrium position. Therefore, a breakage of an upwind mooring line leads to a more severe yaw motion of the platform, resulting in a larger yaw-deviation of the rotor.

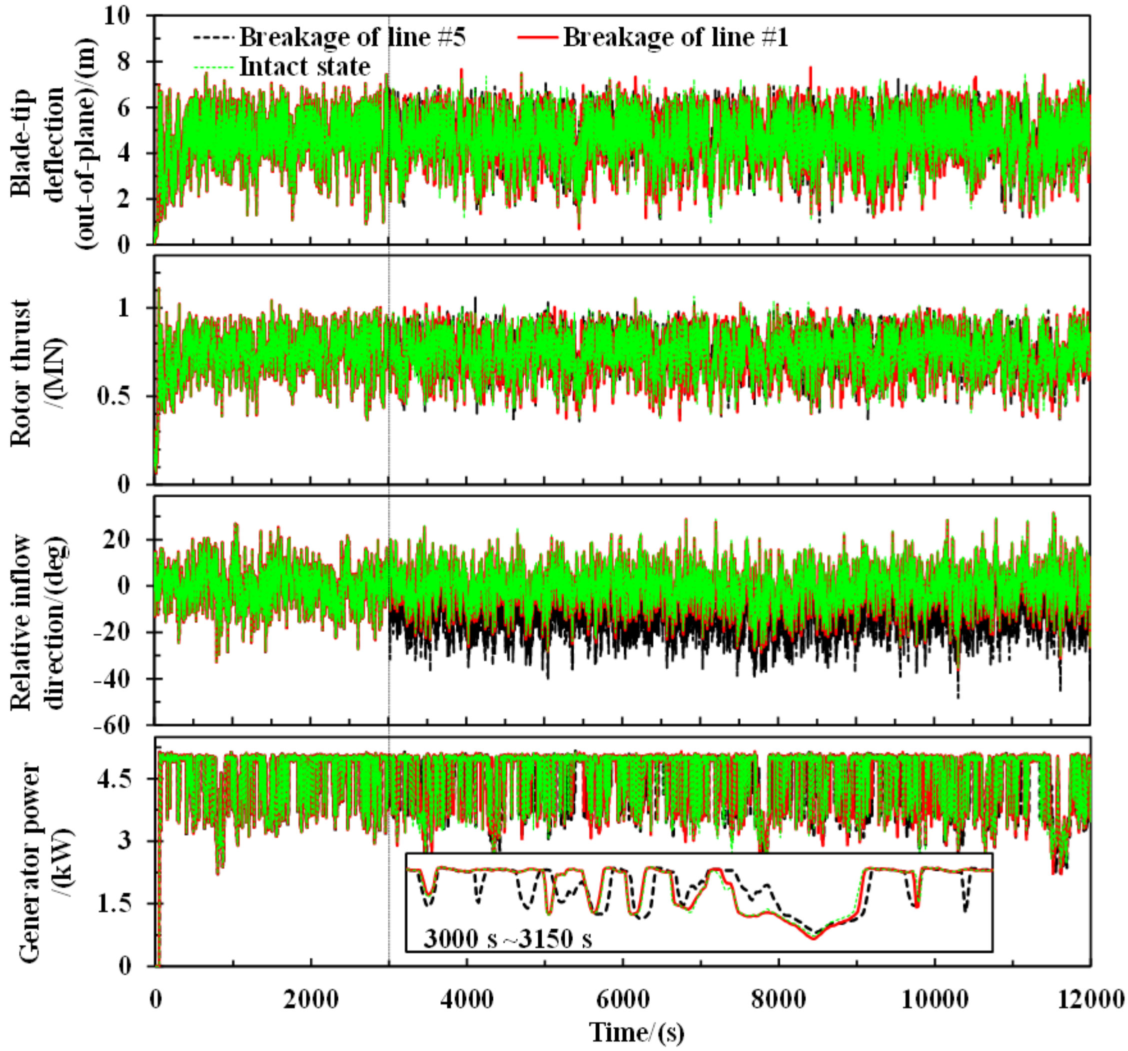

Fig. 7: Rotor dynamic responses under the intact state and mooring breakage conditions

It is observed that the generator power under the breakage scenario of line #5 differs from those of other two cases. This is mainly caused by the large yaw-deviation of rotor due to the platform yaw motion. When mooring line #5 suffers from a breakage, the rotor-nacelle-assemble rotates about the centerline of tower following the platform yaw motion. In this situation, the inflow wind blows towards the rotor with a skew angle, resulting in a slight influence on the aerodynamic performance of the FOWT.

Fig. 8 presents the translational and rotational motions of the platform under the intact state and mooring breakage conditions. The results show that the breakage of mooring line #1 causes insignificant responses on the platform motions with an exception in the yaw. Due to the breakage of mooring line #1, the average value of platform yaw increases from 0.29 degrees to 1.26 degrees and the maximum yaw angle of the platform increases from 0.71 degrees to 3.44 degrees. This means that the platform yaw motion is enhanced by around five times after the breakage occurred on mooring line #1. It is noted that there are much larger responses when a breakage occurs on mooring line #5. With a fraction of tension loss on the station-keeping system, the platform drifts to a further position as indicated by the larger surge and sway motions. This is because the large yaw motion induced by the mooring breakage produces a larger lateral component of the aerodynamic loads. Consequently, the platform has a large drift in the sway direction. The average and maximum values of the platform sway are, respectively, 13.6 m and 29.6 m when the breakage occurs on mooring line #5, while the corresponding values for the intact state are 0.01 m and 2.38 m, respectively. The large drifts caused by the breakage of mooring line #5 are anticipated to increase the tension of the remaining mooring lines placed in the upwind directions.

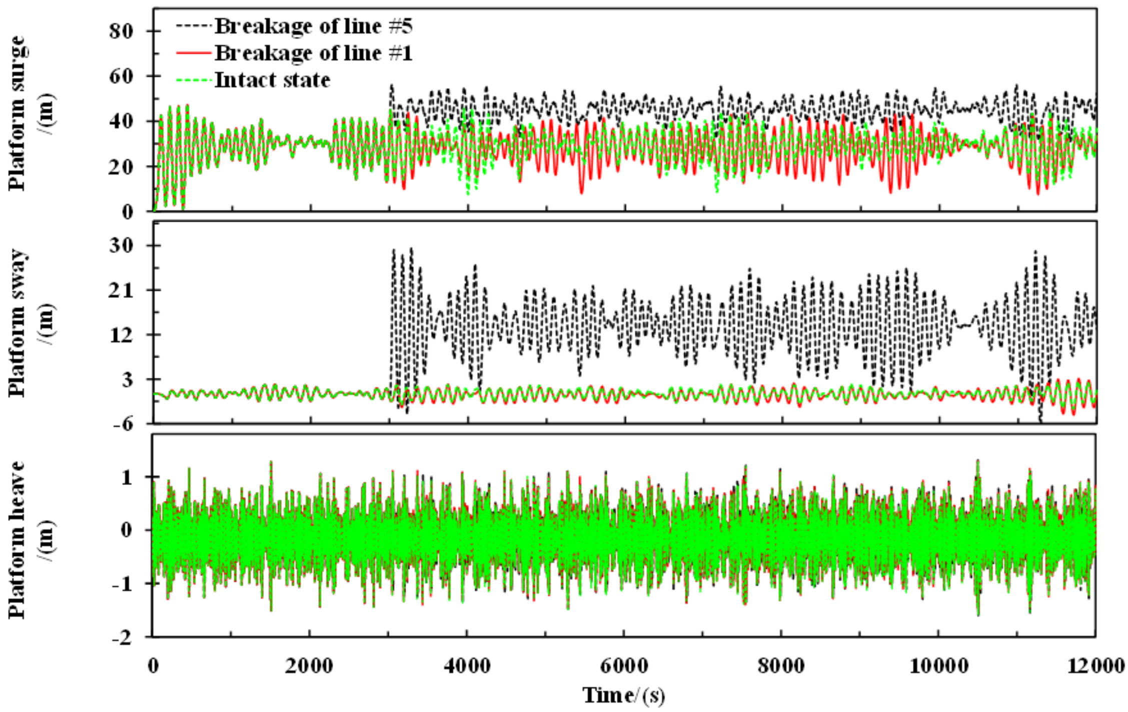

(a) Platform translational motions

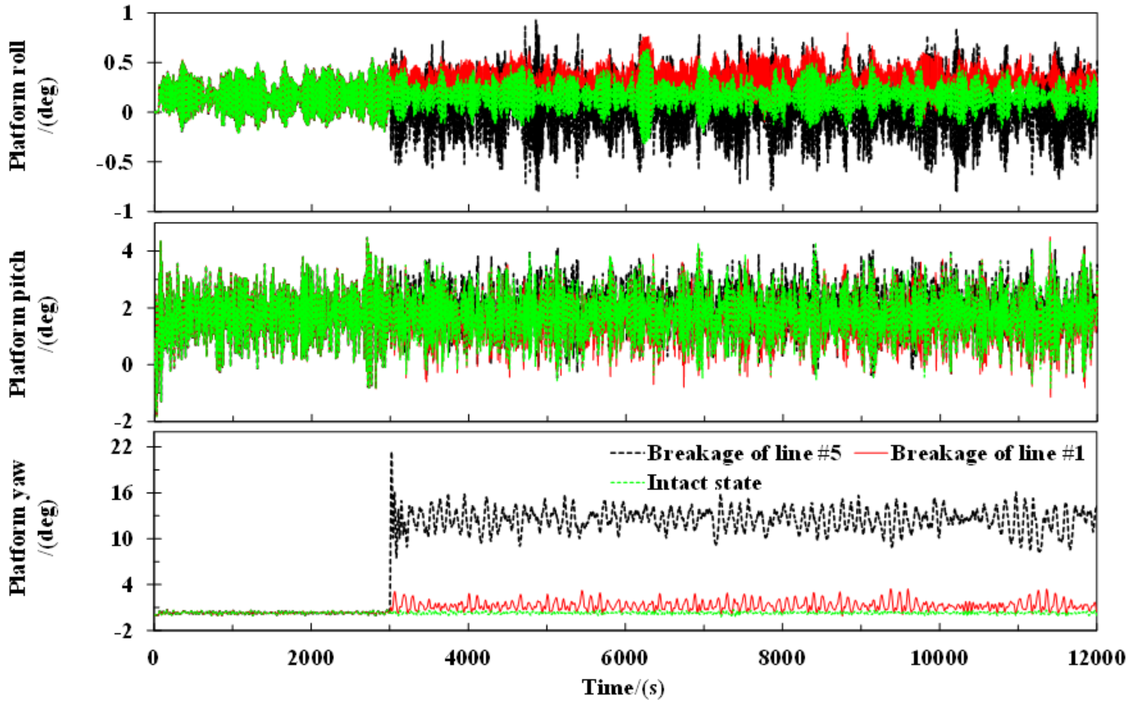

(b) Platform rotational motions

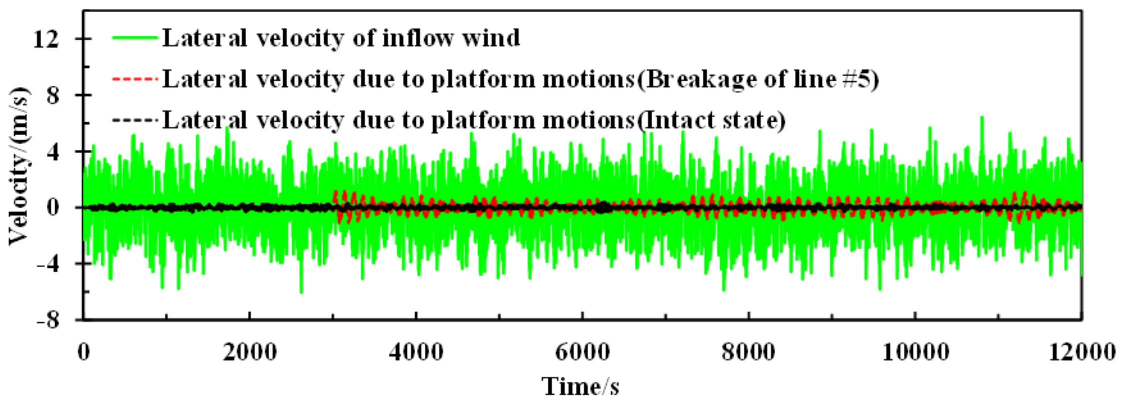

(c) Lateral velocity variations

Fig. 8: Platform motions under the intact state and mooring breakage conditions

It is noted that large sway motion caused by a mooring breakage has a slight influence on the aerodynamic performance of the FOWT as observed from Fig. 7. This phenomenon can be explained by the variation of relative wind speed from two aspects. First, the difference between the wind speeds in two different lateral positions is not significant. Secondly, the lateral component of relative wind speed is still dominated by the inflow wind. Although notable sway and roll motions are caused by a mooring breakage, their contributions to the lateral component of relative wind speed are much smaller than the lateral velocity of the inflow wind, even under the mooring breakage scenarios, as observed from Fig. 8(c). More specifically, the lateral velocity due to the platform's motions under the intact state varies from -0.38 m/s to 0.39 m/s. Under the breakage scenario of line #5, lateral velocity due to platform motions fluctuates within -1.10 m/s ~ 1.20 m/s, while the lateral inflow wind speed fluctuates from -6.05 m/s to 6.43m/s. Therefore, the sway motion of the platform has an insignificant effect on the aerodynamic performance of the wind turbine.

The results presented in Fig. 8-(b) show that the platform pitch is insensitive to the breakage of a mooring line, though minor differences between the results of the intact and broken mooring scenarios are observed. Nonetheless, platform roll and yaw motions are increased by a mooring breakage. The maximum platform yaw increases from 0.29 degree to 21.44 degrees when the mooring line #5 is broken. Meanwhile, the fluctuation range of roll is widened from -0.33 ~ 0.63 degree to -0.81 to 0.93 degree. The enhancement on the platform roll is attributed to the increase in lateral component of the aerodynamic loads under a large yaw condition.

Fig. 9 presents the fairlead tension of the remaining mooring lines when a breakage occurred. Compared to the results of the intact state, the fairlead tension of each of the remaining mooring lines increases slightly when mooring line #1 is broken. The enhancement of the tension due to the breakage of mooring line #1 is negligible. However, the breakage on mooring line #5 leads to significant changes in the tensions of the remaining mooring lines. Specifically, minor reductions are produced in the tension of a downwind mooring line. The average value decreases from 239 kN to 204 kN and the maximum value reduces from 270 kN to 245 kN with regards to the fairlead tension of mooring line #2. Similar reductions in the tension of mooring line #8 are observed. However, on the contrary, the breakage of line #5 causes significant increase in the tension of mooring lines #4 and #6 that are placed in the upwind direction. The average tensions of mooring lines #4 and #6 increase by 30.7% and 62.8 %, respectively. The maximum tensions are increased by 20.7% and 156.1% for mooring lines #4 and #6, respectively. These observations indicate that the breakage of an upwind mooring line produces more stresses on the station-keeping system compared to a scenario in which a breakage occurs on the downwind mooring line. The reason is that the platform drift due to wind loading keeps the upwind moorings taut and the downwind moorings loose. Once a breakage occurs on an upwind mooring, the platform will drift further to a new position that leads to a tauter state for the remaining upwind moorings and a more loose state for the downwind moorings.

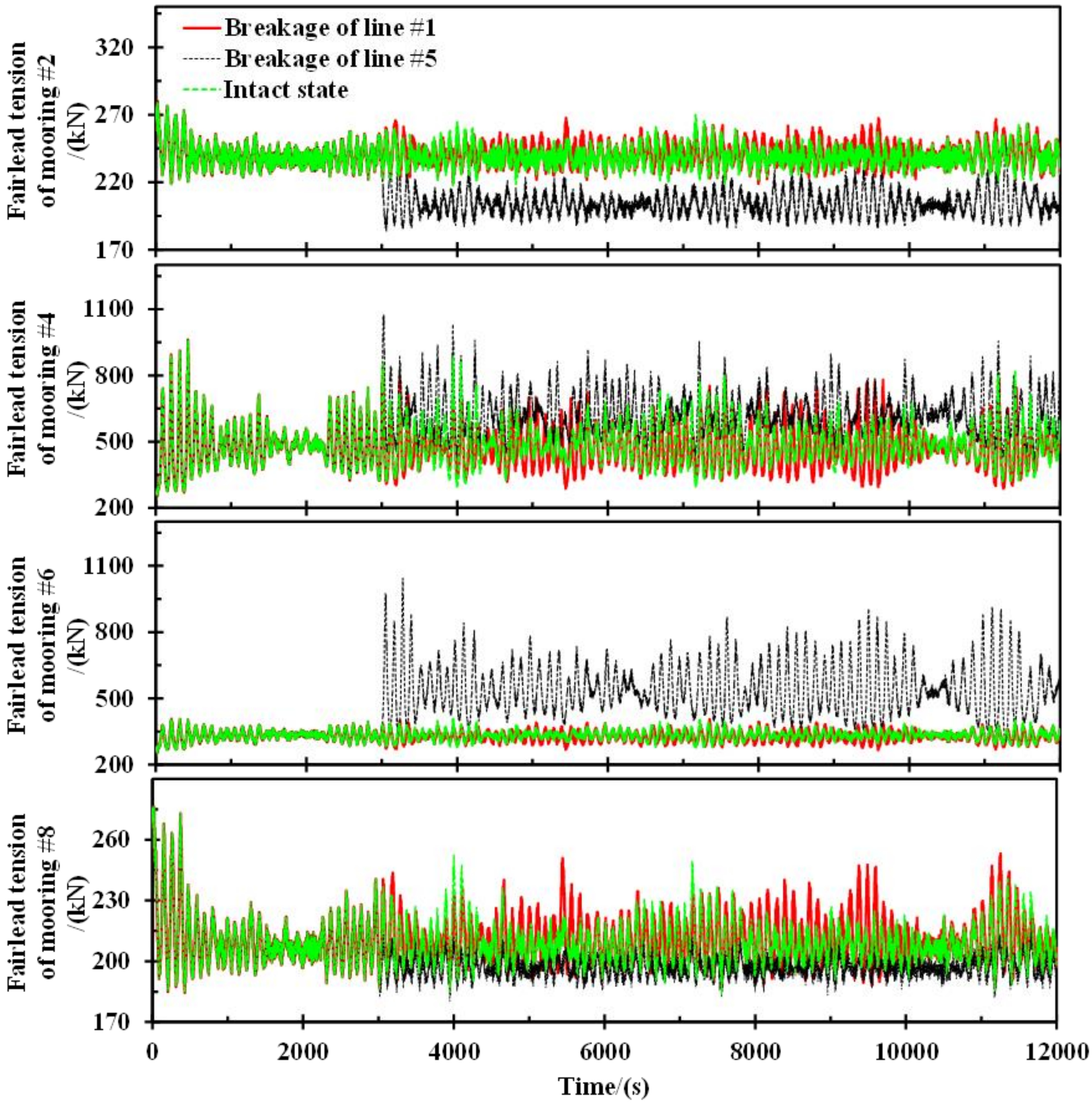

Fig. 9: Fairlead tension of the remaining moorings

The average and maximum tensions in the remaining moorings under different breakage conditions are presented in Fig. 10. As can be seen, the breakage of a mooring line produces insignificant changes in the tensions of mooring lines #2 and #8. This implies that the downwind mooring lines are insensitive to a failure on the mooring system. However, the tension of an upwind mooring line is significantly influenced by the mooring breakage, especially in the case of mooring line #6. For instance, when the breakage occurs on mooring line #5, the mean tension in line #6 increases from 333.1 kN to 542.3 kN and the maximum tension increases from 407.8 kN to 1044.5 kN, reaching 23.6% of the breaking load. This means that the average and maximum tensions are increased by 62.8% and 156.1%, respectively. Its standard deviation is also enhanced by over four times. These results imply that the breakage of mooring line #5 causes mooring line #6 to undertake a much more severe load. Nonetheless, the maximum tension in the mooring lines is much smaller than its breaking load, implying that the mooring system is in a safe situation when a mooring line suddenly fails under the examined operational condition.

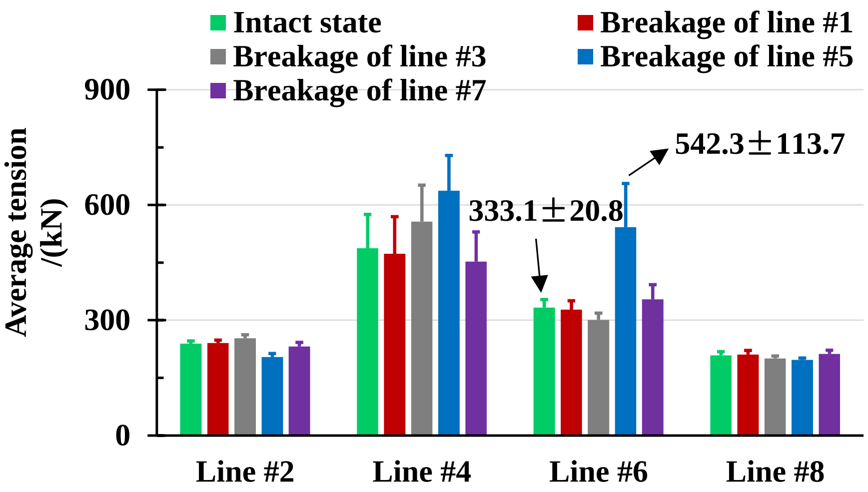

(a) Average tension

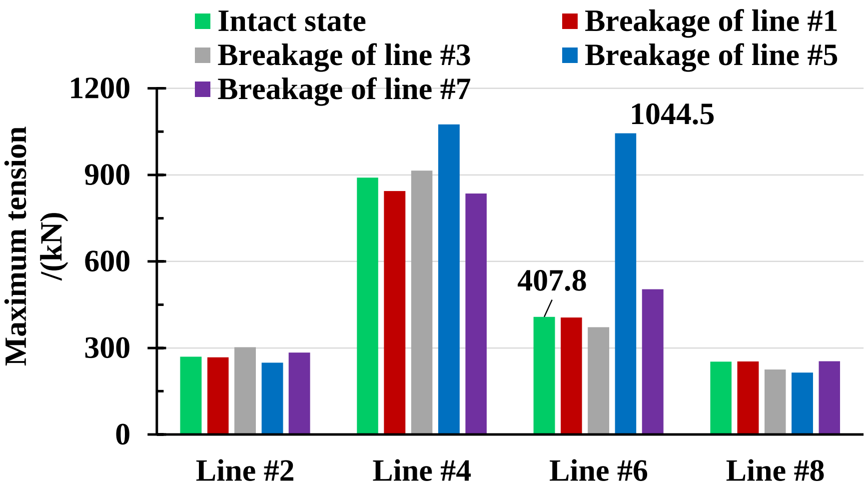

(b) Maximum tension

Fig. 10: Average and maximum tensions of the remaining moorings under different breakage

conditions

4 Effects of the shutdown measure under a mooring breakage scenario

According to the results presented above, the breakage of mooring line #5 leads to the most severe consequences on the FOWT. When a breakage occurs on line #5, the platform has much larger drift motion due to the loss of a fraction of tension of the station-keeping system. As a result of the large drift, the tensions of the remaining upwind mooring lines are significantly increased. Therefore, the shutdown operation of the wind turbine could be used as an efficient measure in moderating the responses of the platform and the mooring system by reducing the driving power of platform drift.

Fig. 11 presents the platform motions under the in-operation and shutdown states when the mooring system is subjected to a breakage on mooring line #5. In the shutdown case, the generator is turned off with a delay of two seconds after the breakage of the mooring line. In the meantime, the blades start the process of pitching to feather. The pitch angle of the blades increases to the feather position (90 degrees) with a pitch rate of 8°/s. The trajectories of the platform under the shutdown and in-operation states are presented in Fig. 12

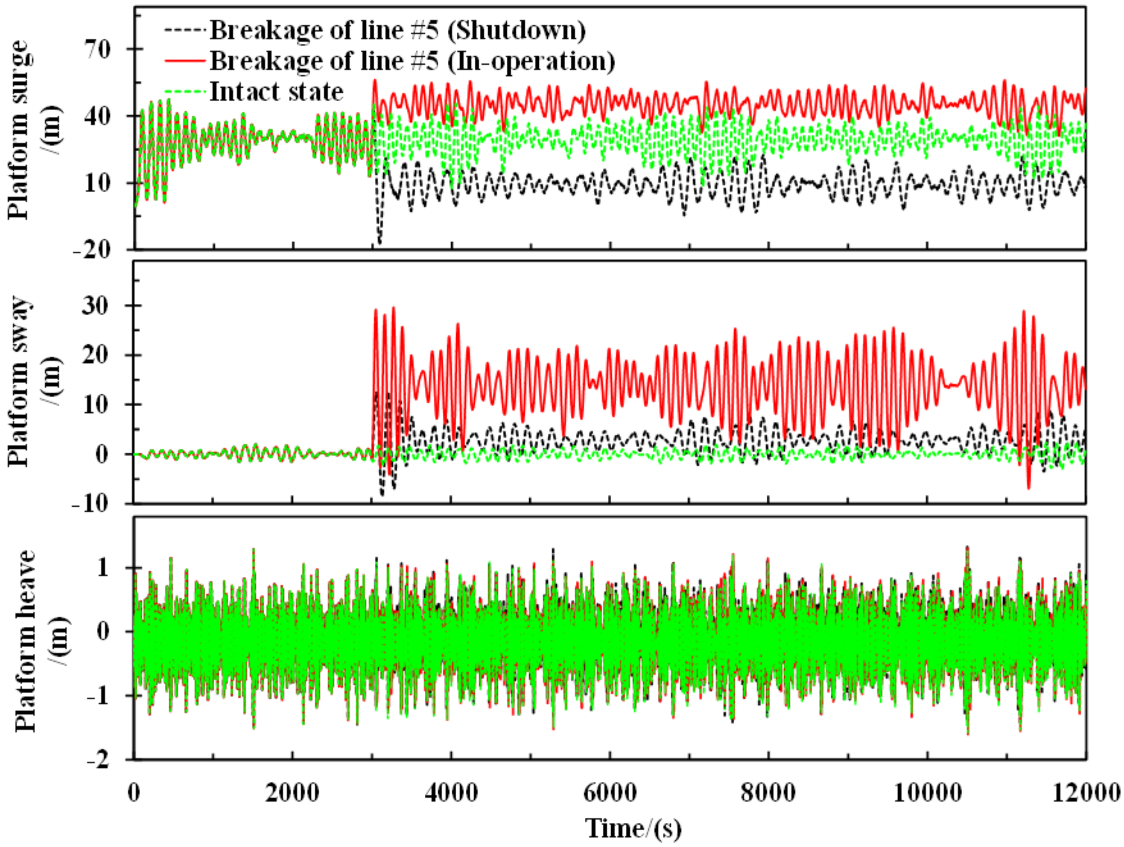

(a) Transitional motions

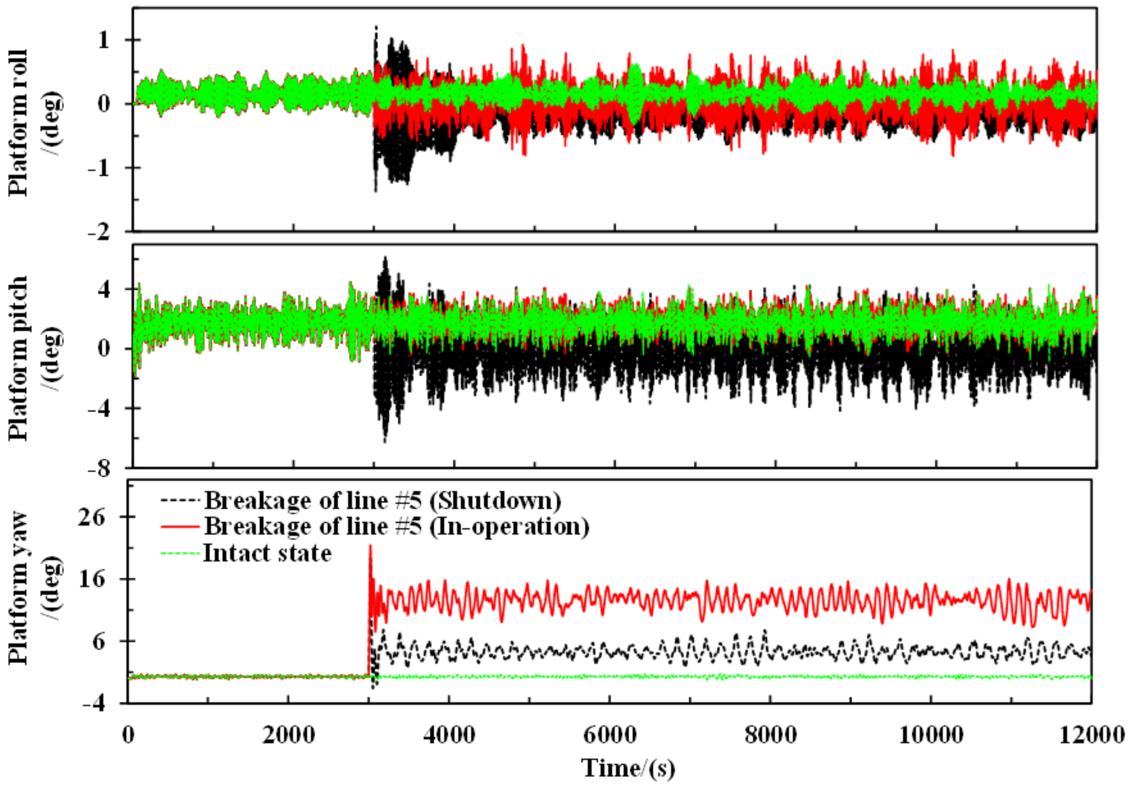

(b) Rotational motions

Fig. 11: Platform motions under the in-operation and shutdown states

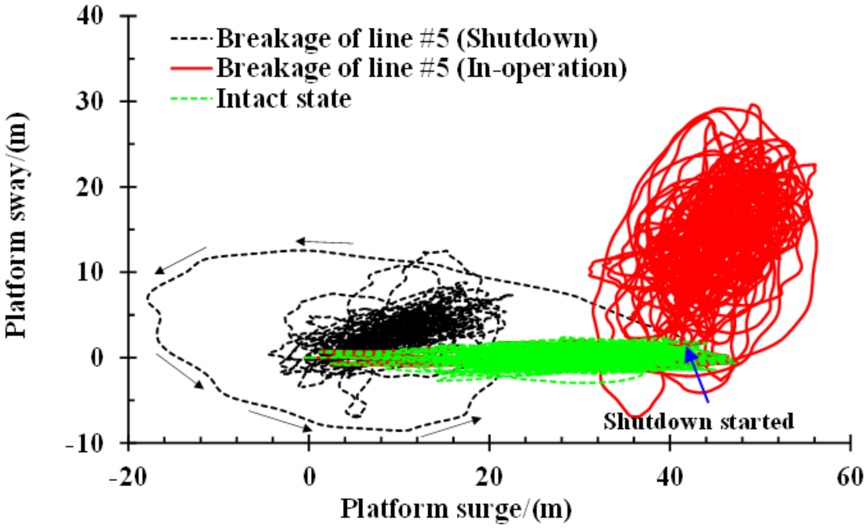

Fig.12: Platform trajectory under the in-operation and shutdown states after a breakage of mooring line

As can be seen from Fig. 11, the platform surge decreases significantly as expected due to the large reduction in aerodynamic loads after the shutdown of the wind turbine. The aerodynamic damping that resists the platform motion to wind is decreased. With the gradual decrease of aerodynamic damping, platform moves towards the upwind direction (minus surge) and then drifts towards the downwind direction until it attains a new equilibrium position as shown in Fig. 12. The variation range of surge under the normal operation state with intact mooring line is [7.5 m, 45.6 m], while the variation range of surge is [31.1 m, 56.2 m] due to the breakage of line #5 and the surge motion varies from -17.9 m to 43.4 m under the shutdown state. After the completion of the transient responses caused by the shutdown measure, the surge fluctuates in a normal variation range similar to that of the intact state. Due to the shutdown of the wind turbine, the platform yaw also decreases to a much smaller level. The average yaw motion is reduced from 12.5 degrees to 4.3 degrees. A similar trend is observed for the platform sway. As discussed previously, a large yaw motion is caused since the restoring stiffness provided by the mooring system is decreased due to breakage of line #5. Under the normal operation state, aerodynamic loads on the blades that deflect asymmetrically because of variations in the rotor-azimuth angle activate the yaw mode of the FOWT. The force component that pushes the FOWT to move along the sway direction is increased due to the large yaw.

As a result, a large swaying motion is produced. However, the shutdown measure significantly decreases the aerodynamic load that is the major source of sway and yaw motions. Therefore, the sway and yaw motions of the platform are reduced by the shutdown measure. However, it is observed that the platform pitch motion varies in a larger range after the shutdown. The variation range is widened from -0.5 ~ 4.2 degrees to -6.2 ~ 6.2 degrees with a 114.1% increase in the standard deviation of platform pitch. The reason is that the aerodynamic damping is significantly reduced when the blades are operating in the feather positions. Consequently, the platform pitch motion fluctuates more severely.

Fig. 13 presents the fairlead tensions of the remaining mooring lines under the in-operation and shutdown states after mooring line #5 is broken. It is found that the fairlead tensions in mooring lines #4 and #6 are significantly reduced due to the emergency shutdown after a breakage of mooring line #5. When the breakage occurs on line #5 and the wind turbine is still in operation, the average and maximum values of the tension in mooring line #4 are 637.3 kN and 1075.1 kN, respectively. The average and maximum values of the tension are 303.4 kN and 748.6 kN, respectively, for the shutdown state. This is because the platform surge is largely decreased due to the reduction in aerodynamic damping after the shutdown. The upwind mooring lines are in a loose state. Similar reduction in the tension of line #6 is achieved, while the average tension falls below the level corresponding to the intact state. It is noted that the shutdown induces minor increases in the tension of mooring line #2 and line #8. More specifically, the maximum tensions in line #2 and line #8 under the normal operation state are 248.9 kN and 214.6 kN, respectively, while the corresponding values are increased to 313.0 kN and 383.8 kN. This is because the platform moves towards the upwind direction due to the reduction of aerodynamic damping. Accordingly, the downwind moorings are certainly stretched and bearing larger tensions. However, the increase in tension of the downwind mooring lines is much smaller than the reductions achieved in the upwind mooring lines. The shutdown measure is beneficial in guaranteeing the operational safety of the FOWT with a sudden breakage of the mooring line.

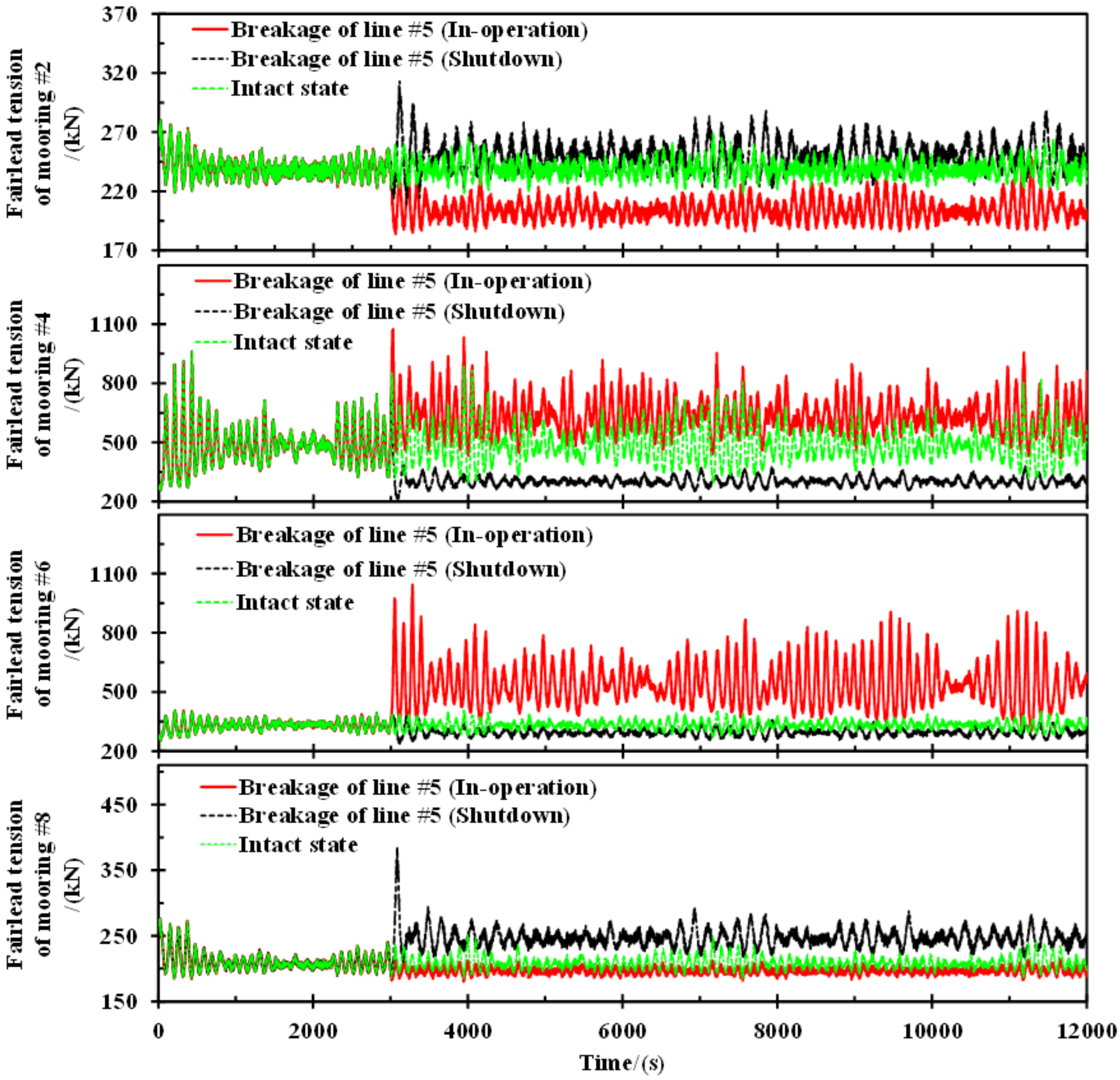

Fig. 13: Fairlead tension of the remaining mooring lines under the in-operation and shutdown states after mooing line #5 is broken

5 Mooring breakage effects under survival condition

The results presented in the previous section indicate that the remaining mooring lines do not have the risk of failure when a mooring line suddenly breaks under the rated environmental condition. In order to further confirm the survivability of the mooring system, a mooring breakage analysis under an extreme condition needs to be performed. It is noted that the ITI barge concept was initially designed for a wind-wave hybrid energy system. For the FOWT where wave energy convertors (WECs) are not installed to absorb the incident wave energy, the barge platform will experience excessive pitch motion under a harsh wave condition as revealed by Jonkman [23]. In addition, the coupling between aerodynamic loads on the blades and platform responses induced by wave loading triggers roll and yaw modes of the platform. Therefore, the platform was suggested to be installed in a site with moderate met-ocean environments if WECs are not considered. The measured met-ocean data at a site located off the northern Scotland [35] is used to define the extreme environmental condition. The significant wave height of the 50-year return extreme condition is 4.3 m and the corresponding spectral peak period is 10.3 s. The average wind speed at the hub-height is 50 m/s. The wind turbine is under the parked state to dissipate the extreme aerodynamic loads by setting the blade-pitch to 90 degrees.

The platform motions of the FOWT with intact and broken mooring lines under the extreme condition are presented in Fig. 14. Since the wind turbine is under the parked state, the aerodynamic damping resisting the platform motion is small. The platform surge has a very large variation range due to the incident wave loading. Due to the absence of aerodynamic damping, the platform also pitches in a large amplitude that is close to 20 degrees. When a mooring breakage occurs, the yaw stiffness provided by the mooring system is decreased, resulting in a large yaw motion as observed from Fig. 14(b). At this stage, the misalignment of the wave loading from the symmetry plane of the platform activates the roll mode. This problem is more significant when line #7 is broken. Large platform motions are anticipated to produce more severe loads in the mooring lines.

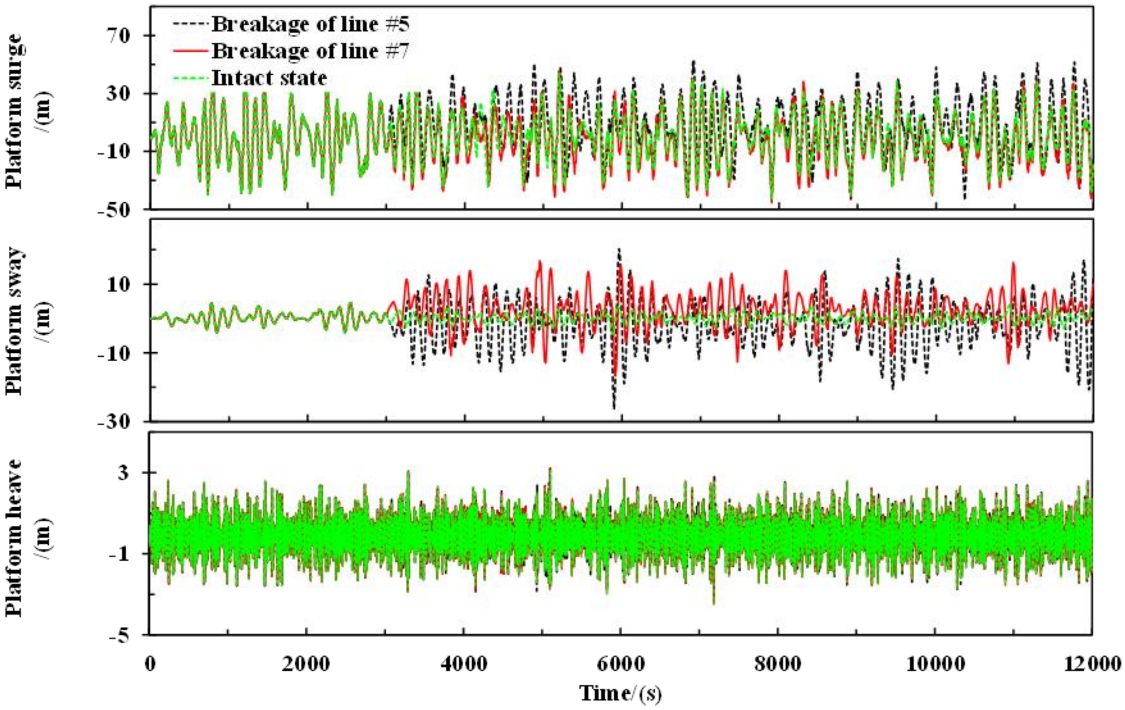

(a) Platform translational motions

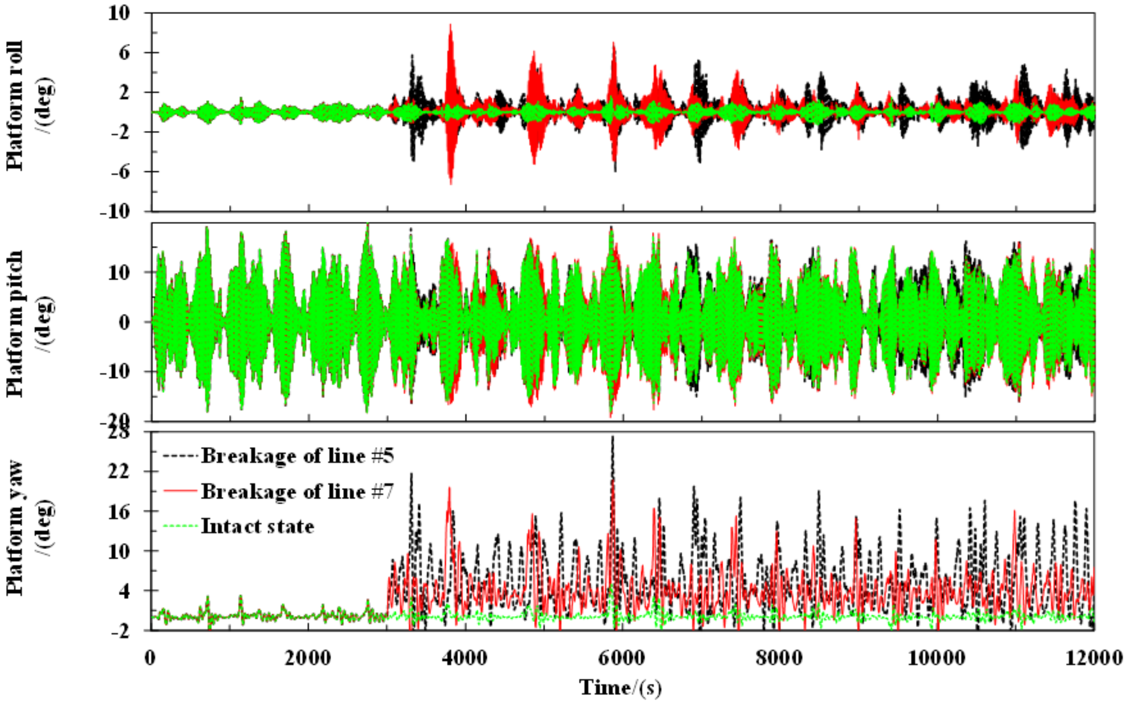

(b) Platform rotational motions

Fig. 14: Platform motions of the FOWT with the intact and broken mooring lines under the extreme environmental conditions

Fig. 15 presents the fairlead tension in the remaining mooring lines when a mooring line suffers from a sudden failure. It is observed that the tension in each mooring line varies severely even under the intact state due to large platform motions. The mooring breakage enhances the dynamic effects of the mooring system as confirmed by the larger tension peaks as observed in Fig. 15. The phenomenon is more obvious for mooring line #4 when a breakage occurs on line #5. The maximum tension in line #4 is 1087.5 kN after the breakage of line #5, while the maximum tension in line #4 under the intact state is 767.8 kN.

Fig. 16 presents the statistical tension of the examined cases. It is found that the tension in line #4 exceeds 1000.0 kN when line #3 fails suddenly. The maximum tensions in other cases are smaller than 900 kN. This means that the tension in these mooring lines under a mooring breakage scenario has not reached a quarter of the breaking load. The mooring system is not at the risk of progressive failure under the examined extreme condition when a mooring is subjected to a sudden breakage.

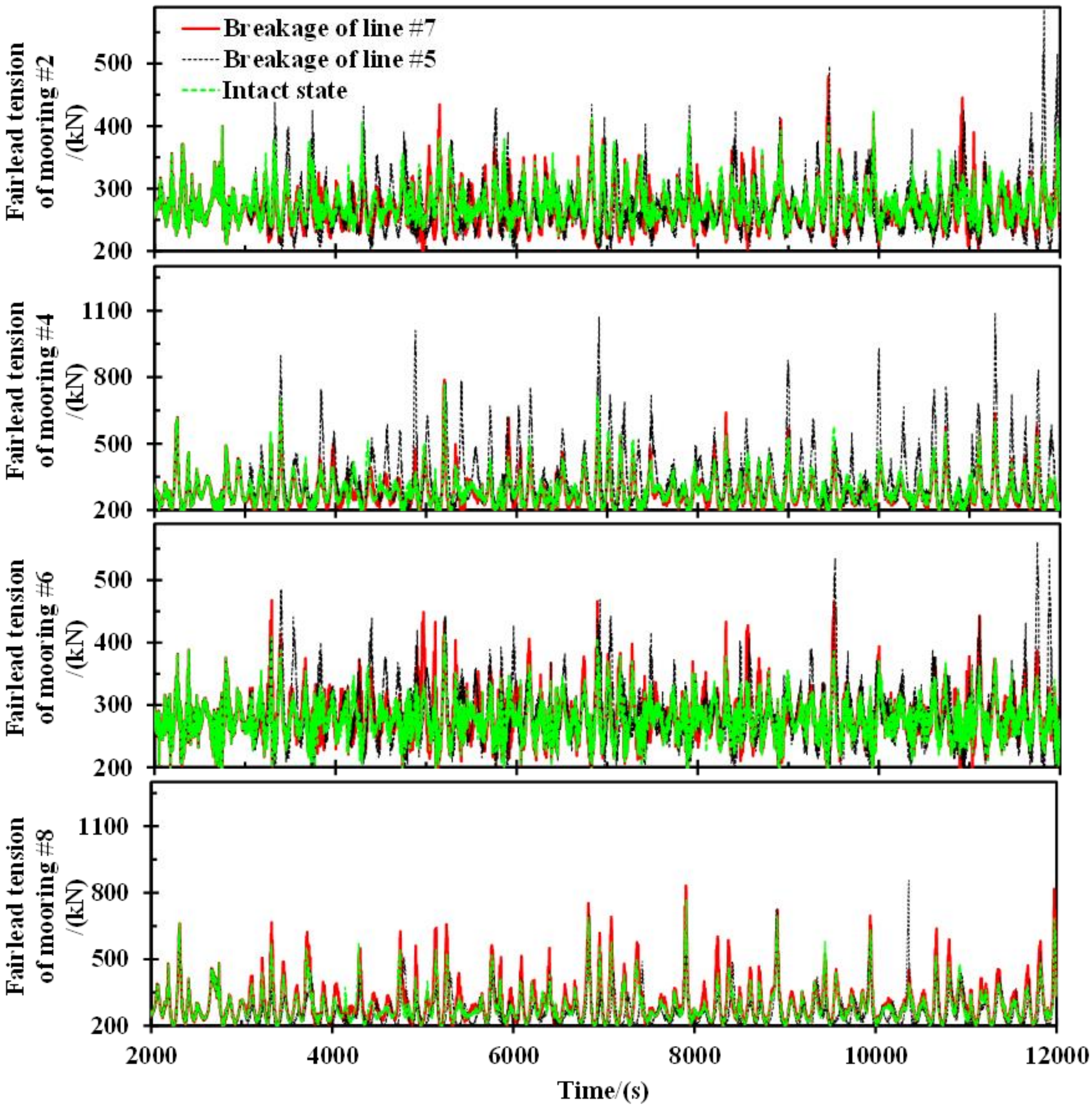

Fig. 15: Fairlead tension in the remaining mooring lines under intact and broken mooring

states

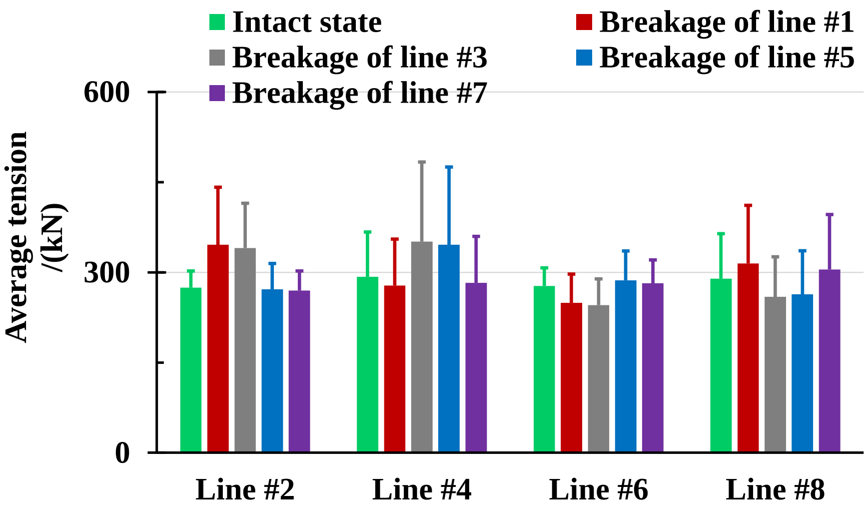

(a) Average tension

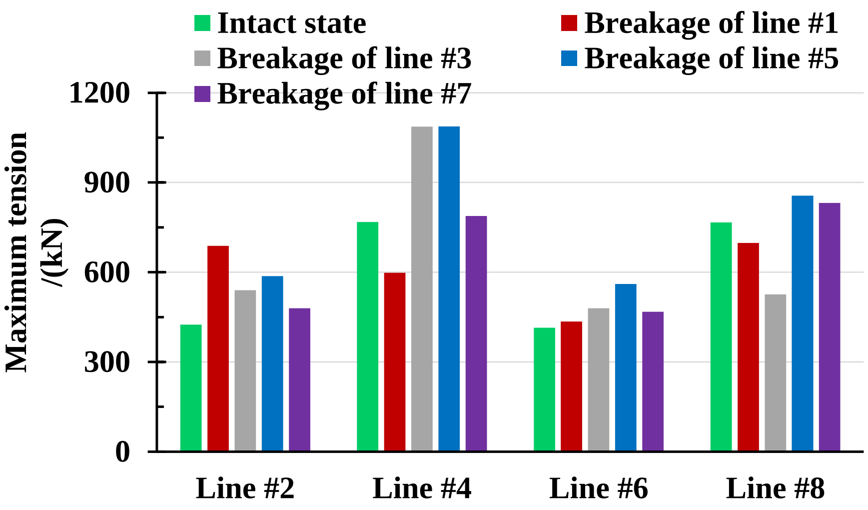

(b) Maximum tension

Fig. 16: Statistical tension in the remaining moorings under the examined extreme condition

6 Conclusions

This paper has investigated the dynamic behaviors of a barge-type 5 MW FOWT subjected to a sudden mooring breakage. A fully coupled aero-hydro-servo-elastic tool (F2A) is developed to conduct the simulations. The nonlinear dynamics of the mooring system with a broken line under normal operation and emergency shutdown conditions are examined for the rated environmental condition. In addition, the survivability of the FOWT subjected to a mooring breakage under an extreme condition is investigated. The effects of the emergency shutdown following the mooring breakage are investigated and discussed. The main findings of this study are summarized as follows:

(1) An original coupling framework (F2A) based on AQWA and FAST is developed and implemented. The dynamic responses of the NREL 5 MW barge FOWT under a turbulent wind combined with a regular wave are obtained by F2A and then compared to the results predicted by OpenFAST. The good agreements between the results have validated the accuracy and credibility of F2A in performing fully coupled analysis of FOWTs.

(2) The aerodynamic performance of the FOWT is insensitive to the mooring breakage, although a relatively larger yaw-deviation of the rotor is caused. The breakage of a mooring line leads to notable changes in the platform sway and yaw motions. The maximum value of platform yaw is increased by around five times due to the breakage of an upwind mooring line.

(3) The tensions of the remaining mooring lines are significantly enhanced by the mooring breakage. In the scenario with an upwind mooing breakage, the tension in the remaining mooring has an increase of 156% in its maximum value and a growth of 20.7% in the average value under the rated condition. It is noted that the maximum tension in the mooring lines under the examined rated and extreme conditions is smaller than a quarter of the breaking load, implying that the mooring system is not at risk of a progressive failure following a mooring breakage.

(4) The emergency shutdown following a mooring line breakage decreases the platform drift distance. The platform surge fluctuates in a normal variation range similar to that of the intact state after the completion of the transient behaviors caused by the shutdown measure. Significant reductions are achieved in the platform sway and yaw motions. The variation range of the platform pitch is enlarged by 162% due to the absence of aerodynamic damping when the FOWT is fully shutdown.

(5) With the rapid decrease in aerodynamic damping during the shutdown period, the platform moves towards the upwind direction, resulting in minor enhancements and significant

reductions in the tensions of downwind and upwind mooring lines, respectively. The shutdown measure is beneficial in ensuring the operational safety of the FOWT subjected to a sudden breakage of a mooring line.

Acknowledgements

The authors would like to acknowledge the financial support from the European Regional Development Fund (ERDF), Interreg Atlantic Area (grant number: EAPA_344/2016) and European Union's Horizon 2020 research and innovation programme under the Marie Skłodowska-Curie grant agreement no. 730888 (RESET).. This study is also partially supported by the National Natural Science Foundation of China (grant numbers: 51676131 and 51976131), Science and Technology Commission of Shanghai Municipality (grant number: 1906052200) and Royal Society (grant number: IEC\NSFC\170054).

References

[1] International Energy Agency. (2020). Offshore wind outlook 2019. *World Energy Outlook Special Report*, Paris, France.

[2] Yang, Y., Bashir, M., Wang, J., Yu, J., & Li, C. (2020). Performance evaluation of an integrated floating energy system based on coupled analysis. *Energy Conversion and Management*, 223, 113308.

[3] Jonkman, J. M., & Matha, D. (2011). Dynamics of offshore floating wind turbines—analysis of three concepts. *Wind Energy*, 14(4), 557-569.

[4] Zuo, S., Song, Y. D., Wang, L., & Song, Q. W. (2013). Computationally inexpensive approach for pitch control of offshore wind turbine on barge floating platform. *The Scientific World Journal*, 2013, 1-9.

[5] Namik, H., & Stol, K. (2011). Performance analysis of individual blade pitch control of offshore wind turbines on two floating platforms. *Mechatronics*, 21(4), 691-703.

[6] Jonkman, J. (2008). Influence of control on the pitch damping of a floating wind turbine. *46th AIAA Aerospace Sciences Meeting and Exhibit*, Nevada, United States.

[7] He, E. M., Hu, Y. Q., & Zhang, Y. (2017). Optimization design of tuned mass damper for vibration suppression of a barge-type offshore floating wind turbine. P*roceedings of the Institution of Mechanical Engineers, Part M: Journal of Engineering for the Maritime Environment*, 231(1), 302-315.

[8] Hu, Y., Wang, J., Chen, M. Z., Li, Z., & Sun, Y. (2018). Load mitigation for a barge-type floating offshore wind turbine via inerter-based passive structural control. *Engineering Structures*, 177,

198-209.

[9] Yang, J., He, E. M., & Hu, Y. Q. (2019). Dynamic modeling and vibration suppression for an offshore wind turbine with a tuned mass damper in floating platform. *Applied Ocean Research*, 83, 21-29.

[10] Qu, X., Li, Y., Tang, Y., Chai, W., & Gao, Z. (2020). Comparative study of short-term extreme responses and fatigue damages of a floating wind turbine using two different blade models. *Applied Ocean Research*, 97, 102088.

[11] Pham, H. D., Cartraud, P., Schoefs, F., Soulard, T., & Berhault, C. (2019). Dynamic modeling of nylon mooring lines for a floating wind turbine. *Applied Ocean Research*, 87, 1-8.

[12] Siddiqui, N. A., & Ahmad, S. (2001). Fatigue and fracture reliability of TLP tethers under random loading. *Marine structures*, 14(3), 331-352.

[13] Gao, Z., & Moan, T. (2007). Sensitivity study of extreme value and fatigue damage of line tension in mooring system with one line failure under varying annual environmental conditions. *The Seventeenth International Offshore and Polar Engineering Conference, International Society of Offshore and Polar Engineers*, Hawaii, USA.

[14] Yang, C. K., & Kim, M. H. (2010). Transient effects of tendon disconnection of a TLP by hull–tendon–riser coupled dynamic analysis. *Ocean Engineering*, 37(8-9), 667-677.

[15] Kim, M. H., & Zhang, Z. (2009). Transient effects of tendon disconnection on the survivability of a TLP in moderate-strength hurricane condition. *International Journal of Naval Architecture and Ocean Engineering*, 1(1), 13-19.

[16] Yang, C. K., Padmanabhan, B., Murray, J., & Kim, M. H. (2008). The transient effect of tendon disconnection on the global motion of ETLP. *In ASME 2008 27th International Conference on Offshore Mechanics and Arctic Engineering. American Society of Mechanical Engineers*, Estoril, Portugal.

[17] Malayjerdi, E., Ahmadi, A., & Tabeshpour, M. R. (2017). Dynamic Analysis of TLP in intact and damaged tendon conditions. *International Journal of Coastal & Offshore Engineering*,1, 23-33.

[18] Bae, Y. H., Kim, M. H., & Kim, H. C. (2017). Performance changes of a floating offshore wind turbine with broken mooring line. *Renewable Energy*, 101, 364-375.

[19] Li, Y., Zhu, Q., Liu, L., & Tang, Y. (2018). Transient response of a SPAR-type floating offshore wind turbine with fractured mooring lines. *Renewable Energy*, 122, 576-588.

[20] Ma, G., Zhong, L., Zhang, X., Ma, Q., & Kang, H. S. (2020). Mechanism of mooring line breakage of floating offshore wind turbine under extreme coherent gust with direction change condition. *Journal of Marine Science and Technology*, 1-13.

[21] Jonkman, J. M. (2007). Dynamics modeling and loads analysis of an offshore floating wind turbine. *National Renewable Energy Laboratory (NREL), Technical Reports (No. NREL/TP-500-41958)*, Golden, United States.

[22] Jonkman, J. M., & Buhl Jr, M. L. (2005). FAST user's guide. *National Renewable Energy Laboratory (NREL), Technical Reports (No. NREL/EL-500-38230)*, Golden, United States.

[23] Jonkman, J. M. (2007). Dynamics modeling and loads analysis of an offshore floating wind turbine. *National Renewable Energy Laboratory (NREL), Technical Reports (No. NREL/TP-500-41958)*, Golden, United States.

[24] Ma, Y., Hu, Z. Q., & Xiao, L. F. (2014). Wind-wave induced dynamic response analysis for motions and mooring loads of a spar-type offshore floating wind turbine. *Journal of Hydrodynamics*, 26(6), 865-874.

[25] Jeon, S. H., Cho, Y. U., Seo, M. W., Cho, J. R., & Jeong, W. B. (2013). Dynamic response of floating substructure of spar-type offshore wind turbine with catenary mooring cables. *Ocean Engineering*, 72, 356-364.

[26] Karimirad, M. (2013). Modeling aspects of a floating wind turbine for coupled wave–wind-

induced dynamic analyses. *Renewable energy*, 53, 299-305.

[27] Hall, M., Buckham, B., Crawford, C., & Nicoll, R. S. (2011). The importance of mooring line model fidelity in floating wind turbine simulations. *In Oceans'11 MTS/IEEE Kona Conference, Institute of Electrical and Electronics Engineers*, Hawaii, USA.

[28] Hall, M., & Goupee, A. (2015). Validation of a lumped-mass mooring line model with DeepCwind semisubmersible model test data. *Ocean Engineering*, 104, 590-603.

[29] ANSYS. (2013). AQWA theory manual. Canonsburg, United States.

[30] Yang, Y., Bashir, M., Michailides, C., Li, C., & Wang, J. (2020). Development and application of an aero-hydro-servo-elastic coupling framework for analysis of floating offshore wind turbines. *Renewable Energy*, 161, 606-625.

[31] Jonkman, J., & Musial, W. (2010). Offshore code comparison collaboration (OC3) for IEA Wind Task 23 offshore wind technology and deployment. *National Renewable Energy Laboratory (NREL), Technical report (No. NREL/* TP-5000-48191*)*, Colorado, United States.

[32] Robertson, A. N., Wendt, F., Jonkman, J. M., Popko, W., Dagher, H., Gueydon, S., ... & Soares, C. G. (2017). OC5 project phase II: validation of global loads of the DeepCwind floating semisubmersible wind turbine. *Energy Procedia*, 137, 38-57.

[33] Yang, Y., Bashir, M., Wang, J., Michailides, C., Loughney, S., Armin, M., ... & Li, C. (2020). Wind-wave coupling effects on the fatigue damage of tendons for a 10 MW multi-body floating wind turbine. Ocean Engineering, 217, 107909.

[34] Jonkman, Bonnie J. (2009). TurbSim user's guide: Version 1.50. Jonkman, J. M., & Buhl Jr, M. L. (2005). FAST user's guide. *National Renewable Energy Laboratory (NREL), Technical Reports (No. NREL/TP-500-46198)*, Golden, United States.

[35] Ifremer. Marine Data Portal, French Research Institute for the Exploitation of the Sea, Online: http://data.ifremer.fr/pdmi/portalssearch/main. Data Accessed: January 2019.